ELSEVIER

Frontiers and Advances in

Molecular Spectroscopy

Edited by **Jaan Laane**

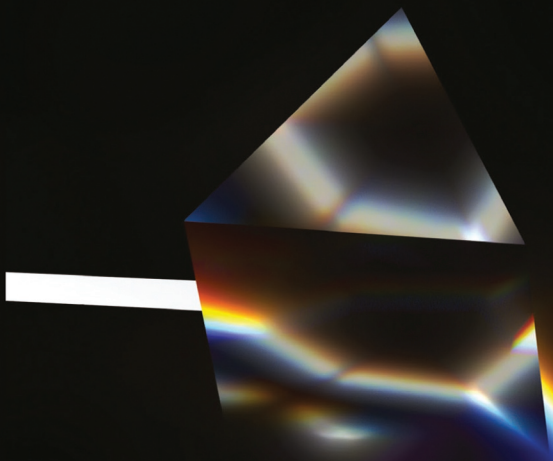

Preface

In 2009, we published the book "Frontiers in Molecular Spectroscopy" containing 19 chapters by eminent authors in the field. From that time, the field of molecular spectroscopy has continued to move forward, and it has been found appropriate to have 10 of the previous chapters that authors discuss their most recent results. In addition, 11 additional chapters will discuss the results from other research groups.

The preface to the previous book began with a historical perspective of spectroscopy, and since the early history has not changed, it will be repeated here:

Although Aristotle recognized that light was necessary for color to exist and Aristophanes made use of lenses before 400 BC, the origins of spectroscopy are perhaps best traced back to Newton's observation of a spectrum obtained from a prism in 1666. A dozen years later, Huygens proposed the wave theory of light. Other developments in optics, physics, and chemistry ensued over the next century, but it was not until 1800 that F.W. Herschel recognized the existence of infrared radiation and 1801 that J.W. Ritter discovered the presence of ultraviolet light. In the next quarter of the century, during which John Dalton proposed the atomic theory, W.H. Wollaston and Josef Fraunhofer observed specific absorption lines and W.H.F. Talbot recognized that different salts yield different colors in flames. In the middle of the 19th century, many researchers including Becquerel, Draper, Kirchhoff, Bunsen, and Angstrom contributed extensively to experimental data and were able to correlate spectral properties to the nature of matter, and in 1873, J.C. Maxwell's equations unifying electricity and magnetism were revealed. In 1885, a Swiss high school teacher, J.J. Balmer, finally achieved a major spectroscopic breakthrough by showing that the wavelengths of the visible spectral lines of atomic hydrogen could be predicted by a mathematical formula. Rydberg and Ritz, among others, soon developed a more universal expression for explaining the atomic spectrum of hydrogen ranging from the infrared region to the ultraviolet region. It was clearly demonstrated that each observed spectral frequency was determined from the difference of two fixed quantities. In 1913, Niels Bohr devised a model of the hydrogen atom based on quantum theory, and this laid the groundwork for understanding atomic spectroscopy.

The pioneering work of Planck, Einstein, de Broglie, Heisenberg, and others finally led to Schrodinger's discovery of the wave equation in 1926, which

today serves not only as the basis for understanding atomic and molecular structure but also as the basis of molecular spectroscopy. Work of R.W. Wood in the United States and A. Smekal in Germany helped pave the way for C.V. Raman's discovery of the effect bearing his name in 1928. A few years later in 1933, C.E. Gleeton and N.H. Williams carried out the first microwave absorption experiments. Meanwhile, infrared absorption had been evolving through the work of William Coblentz, H.M. Randall, Gerhard Herzberg, and others, and by 1950, it had become a major tool for qualitative and quantitative chemical analysis, thanks in part to commercial instruments developed by the Beckman and PerkinElmer companies.

During the last half of the 20th century, the development of both lasers and computers immensely helped to advance the field of molecular spectroscopy. C. Townes, A.L. Schalaw, and T.H. Maiman developed the laser in 1958, and this has led not only to the field of Raman spectroscopy flourishing but also to innovative work in fluorescence spectroscopy and a variety of nonlinear techniques. The commercial availability of Fourier transform infrared (FT-IR) spectrometers from about 1970, based on the Michelson interferometer (1880) and Peter Fellgett's theory (1949), rapidly advanced the field of infrared spectroscopy, including near infrared. Commercial instruments, by Bomem, for example, could cover the range from 3 to 50,000 cm^{-1}, well into the ultraviolet region.

During the 20th century, 22 scientists received Nobel Prizes that can be directly or indirectly related to spectroscopy. Most of them are well-known names, and many have had effects or theories named after them. These include A.A. Michelson, H.A. Lorentz, P. Zeeman (magnetic splitting), J. Stark (electric splitting), C.V. Raman, N.E. Lamb, R.S. Mulliken, G. Herzberg, C.H. Townes, A.L. Schawlow, N. Blombergen (nonlinear optics), and A. Zewail (chemical dynamics using femtosecond lasers).

As is evident from all of this, spectroscopy is arguably the one most important tool that has taught us the most about the nature of atoms and molecules, much of this coming in the 20th century. As we now proceed through the 21st century, it is appropriate to examine where we are today in the development of spectroscopic tools that can provide us further insight in a way that only spectroscopy can do.

The present book starts off with a chapter on processes for selectively preparing vibrationally excited quantum states from Dick Zare's prolific research group. The next two chapters by Isao Noda and Neil Hunt then discuss advances and applications of two-dimensional correlation spectroscopy. The chapter by Laane, Ocola, and Chun reviews work on vibrational potential energy surfaces in ground and excited electronic states, and this is followed by four more chapters on electronic excited states. Michael Schmitt and Chenk-Yiu Ng focus on high-resolution electronic spectroscopy, Yusuke Morisawa, Ichiro Tanabe, and Yukihiro Ozaki describe far-ultraviolet work, and the Takayoshi Kobayashi research group highlights work on ultrafast techniques. The next five chapters all present work utilizing Raman spectroscopy. Jaebum Choo discusses

biomedical applications, and Larry Ziegler describes additional applications of surface-enhanced Raman spectroscopy (SERS). Hiro-o Hamaguchi follows with descriptions of a new chemometrical method, hypothetical addition multivariate analysis with numerical differentiation (HAMAND). The next two chapters from the Marlan Scully and Alexei Sokolov physics research programs present additional applications of Raman spectroscopy. Larry Nafie reviews his many contributions to the field of vibrational optical activity. Three chapters then are devoted to low-frequency applications. Stephan Schlemmer presents microwave work of astrophysical interest, Ralf Ludwig reviews his investigations of ionic liquids using far-infrared spectroscopy, and Walther Caminati and Uwe Grabow present a broader view of recent microwave studies. The Simon North's group discusses spectroscopic applications of velocimetry and thermometry. Two chapters are devoted to matrix isolation studies. Rui Fausto describes the photogeneration of rare molecules, and Bruce Ault also reviews his photochemical studies. The final chapter by Kevin Lehman, who has been a pioneer in the development of cavity ring-down spectroscopy, discusses this field.

Ten of the chapters in this book represent updated results from the same research groups that contributed to the previous *Frontiers* book in 2009. The other 11, described above, present new and different topics. It is worth noting that the previous book contains research summaries that remain timely today even though they have not been updated in this edition. Sir Harry Kroto, Nobel Laureate in 1996 for his work on buckyballs, wrote the first chapter reflecting on his work in the area of microwave spectroscopy. George Thomas and Daniel Nemecek discussed Raman studies of viruses and viral proteins, and H.G.M. Edwards contributed a colorful presentation of the use of Raman spectroscopy to investigate art and archeology. Surface-enhanced Raman spectroscopy (SERS) was covered in two chapters. Philip Bunker and Per Jensen presented an insightful journey into spectroscopy and broken symmetry. Bruce Hudson's chapter focused on vibrational studies using neutron scattering demonstrates, and Frederic Merkt described his work on high Rydberg states.

It is clear that the 20th century was a period of unprecedented advances in molecular spectroscopy. However, there is much yet left to be learned. Hopefully, this book helps to present a broad perspective of the many avenues of work underway in the 21st century. From these and other spectroscopic studies, we will continue to understand our universe at the molecular level even better.

As the editor of this volume, I thank all the authors for their excellent contributions.

Jaan Laane
College Station, TX, United States

Chapter 5

Structures and Dipole Moments of Molecules in Their Electronically Excited States

Michael Schmitt* **and Leo Meerts†**

**Heinrich-Heine-University, Düsseldorf, Germany, †Radboud University, Nijmegen, The Netherlands*

Chapter Outline

Frontiers and Advances in Molecular Spectroscopy. https://doi.org/10.1016/B978-0-12-811220-5.00005-8

1 INTRODUCTION

Dipole moments are a measure for the charge separation in a molecule. They are a vector quantity, with the direction of the vector defined from the positive to the negative center of charge. The dipole moment of molecules in their electronically excited states may differ considerable from the ground state values both in magnitude as in direction, due to the different electron distribution in the excited state. This light induced change of the dipole moment may trigger solvent reorientation or relaxation of a solute, or it might cause reorientation of the local protein surrounding of an electronically excited aromatic amino acid. Also the conformations of flexible biomolecules like, e.g., peptides depend on the relative orientations of the backbone dipole moments, the α-helix being the consequence of aligned microscopic dipole moments of the peptide bonds [1, 2]. The conformations might be subject to geometry changes upon the changed dipolar interactions between the different moieties after electronic excitation.

Furthermore, the knowledge of dipole moments of molecules in their electronically excited states is an indispensable prerequisite for the interpretation of resonance energy transfer processes like Förster Resonant Energy Transfer (FRET) [3, 4] and for molecular excitonic interactions [5], which are the basis for the understanding of energy and charge transport phenomena.

While the determination of permanent dipole moments of molecules in their electronic ground state is straightforward[1], excited state dipole moments pose much more experimental problems. Several routes to excited state dipole moments in solution exist, which will be shortly resumed here. These methods employ spectral changes in solution, which comprise

- the application of solvent induced shifts of emission and/or absorption spectra of the substance under consideration (solvatochromism)
- the effect of temperature on the electric properties of the solvent and resulting from this on the spectra (thermochromism)
- the influence of an external electric field on the absorption properties of the substance in solution (electrochromism)
- the influence of an external electric field on the fluorescence anisotropy of the substance in solution

A more direct method employs gas phase spectroscopy, based on the influence of external electric fields on the positions of single rovibronic transitions through the Stark effect [9]. While the former techniques have the advantage of being experimentally less demanding, they lack accuracy for several reasons, which will be discussed in the following. However, all effects, including those in solutions, are finally based on the Stark effect. For electrochromism and Stark

1. Most reliable values of molecular dipole moments in the ground state comprise spectroscopic techniques like microwave spectroscopy using a resonant cavity [6, 7] and molecular beam electric resonance [8].

measurements this field is applied externally, for solvatochromic measurements, the solvent cage of the solvent itself is the source of the electric field.

Historically, excited-state dipole moments have been determined from solvatochromic shifts in solvents of different static dielectric constants [10, 11] or from electro-optical absorption measurements [12, 13]. The evaluation of excited state dipole moments from solvatochromic shifts is based on the application of the so called Lippert-Mataga equation [14, 15]. The derivation of this equation is based on Onsager's reaction field [16], which assumes the fluorophore to be a point dipole, which is located in the center of a spherical cavity. The cavity of radius a is formed by the homogeneous and isotropic solvent with the permittivity ϵ. The molecular dipole moment of the solute induces a dipole in the homogeneous solvent. This (reaction) dipole is the source of an electric field, which interacts with the molecular dipole, leading to a stabilization. This model already defines the limits of the method, since the original Lippert-Mataga theory does not account for nonspherical cavities, expanded dipoles in the cavity, specific interactions between the solute and the solvent like hydrogen bonds, etc., and reorientation of the molecular dipole upon electronic excitation. Numerous improvements to the basic Lippert-Mataga theory have been introduced over the years, like the utilization of multiparameter solvent polarity scales, which quantitatively reproduce solvent-solute interactions. These interactions are modulated through linear solvation energy relationships [17, 18]. An improved model by Abe also allows for a determination of the angle θ between the ground and excited state dipole moments [19]. All improvements add a several new parameters, which are mainly empirical, like scaling factors for the solvent hydrogen solvent bond donor acidities and basicities, empirical polarity parameters of the solvents, and the volume variation of cavity with solvent polarity to account for nonspherical cavities [20].

Therefore the method of using solvent shifts arouse criticism by Lombardi [21, 22], who compared so determined excited state dipole moment changes with those from high resolution gas phase Stark effect measurements. In some cases the condensed phase values exceeded the more precise gas phase values by an order of magnitude. The main reason for this strong discrepancy is the approximative nature of the field induced perturbations in case of the strong fields, exerted by the solvents. Due to the small size of the cavity, which has atomic dimensions, the field strengths are very large. In the case of aniline, the cavity volume is about 37 $Å^3$ equivalent to a cavity radius of 3.33 Å. With a reaction dipole of 1.3 Debye, a field strength in the cavity of 10^8 V/cm is reached[2]. This strong field couples especially energetically close-lying electronically excited states, leading to an effective dipole moment, which is a combination of the excited-state dipole moments of the coupled states as well as the transition moment between these two states [22]. This effect can be viewed as a

2. Rotationally resolved Stark spectroscopy uses electric field strengths of 1–10 kV/cm, sometimes even 100 V/cm a sufficient to determine dipole moments.

field induced dipole moment borrowing from the state with the larger dipole moment. Especially for substituted indoles, for which the energetic distance between the lowest electronically excited singlet states is small, this perturbation plays a large role. The use of thermochromic shifts of fluorescence spectra for the determination of S_1-state dipole moments [23, 24] yields more reliable values, than the aforementioned methods, because artificial effects by the use of different solvents are excluded.

Since the interaction of the solvent permanent dipole moment with the induced dipole moment of the solute depends on the polarizability of the solute, excited state dipole moments, which have been determined from solvatochromic shifts may differ from solvent to solvent. The permanent dipole moment of aniline in its lowest electronically excited singlet state has been determined from a variety of the above-mentioned methods. Lombardi used the optical Stark effect on the vibronic contour of the electronic origin and reported a value of 2.38 ± 0.15 D in the gas phase [25]. Later, Lombardi detected electric field induced perturbations from a higher-lying more polar state, which shifted the value of the dipole moment to 2.45 ± 0.15 D [26]. The dipole moment of the perturbing state was determined to be 6.0 D [27]. From high resolution Stark spectroscopy in the group of Pratt a gas phase value of 2.8 ± 0.15 D was determined [28]. In solution the dipole moments for the S_1-state are rather different. From solvent shifts of absorption and fluorescence spectrum a value of 5 D was found [29]. The solvatochromic shift method of Bakshiev's and Kawski-Viallet's correlations gave values of 4.91 and 4.93 D, respectively [30], while the evaluation of absorption and fluorescence solvatochromic shifts with a modified approach, which makes no assumption about the angles between the ground state and excited state dipole moment vectors, resulted in an S_1-state dipole moment of 5.38 D [31]. On the other hand, Prabhumirashi [32] obtained a value for $\mu(S_1)$ of 2.12 D from solvatochromic shifts in solution, and Kawski et al. [23] a value of 2.38 D from thermochromic shifts.

There are at least five main reasons for the large discrepancies of S_1 state dipole moments of aniline determined in solution from one of the above methods:

- **(i)** The Onsager radius is neither well known nor well defined, but enters the Lippert-Mataga equation with cubic power.
- **(ii)** In some of the studies the Onsager reaction field for a polarizable point dipole of the solute has not been utilized (e.g., in [29]) but instead a correlation function which contains only the index of refraction and dielectric constant of the solvents.
- **(iii)** The inherently low resolution in solution makes the determination of spectral shifts cumbersome.
- **(iv)** The large field strengths in solution lead to perturbative state mixing with nearby electronic states of different dipole moment.
- **(v)** For molecules in which the direction of the dipole moment changes upon excitation an additional difficulty arises.

This confusing situation is tellingly summarized by Lombardi [33]: "*It is unfortunate so much energy has been expended in solvatochromic studies determining excited state dipole moments, many of which are highly suspect. It would be far preferable if we would treat the gas phase results for what they probably are the most accurate current technique for determining molecular dipole moments of an isolated molecule, and to expend some energy instead utilizing the solvatochromic shifts as a good way to determine the effect of solvents on electronic reorganization upon excitation by judicious comparison with the gas phase results.*"

However, the most reliable values for dipole moments of ground and electronically excited states are obtained from high resolution gas phase electronic Stark spectra, since the dependence of the frequency shift of individual rovibronic lines from the electric field strength yields immediately the dipole moment in ground and excited state. Moreover, not only the absolute value of the total dipole moment can be determined but also the Cartesian components of the dipole moment in both electronic states. This is especially important in cases in which the orientation of the dipole moment changes upon electronic excitation. The first determination of excited state molecular dipole moment of a small polyatomic molecule goes back to Freeman and Klemperer, who determined the excited state dipole moment of formaldehyde [34]. Hese and co-workers [35], Pratt and co-workers [28], and later the group of Schmitt [36] used the Stark effect in rotationally resolved electronic spectra of large polyatomic molecules and molecular clusters to determine the dipole moments in the ground and the lowest electronically excited singlet states. Apart from these spectroscopic techniques a time domain approach to excited state dipole moments in the gas phase is used in coherent beat techniques with a Stark field, pioneered in the groups of Sodeik [37], Zare [38], Huber [39], and Tanaka [40].

2 PERMANENT DIPOLE MOMENTS AND TRANSITION DIPOLES

The dipole moment is only one term in the general expansion of the potential energy of known charge distribution outside the region where the charges are. In order to expand the potential energy into a series, the reference point P has to be at infinity, an approximation, which is made implicitly, but which has to be questioned in several cases. The multipole expansion of the potential energy $V(r)$ gives:

$$V(r) = \frac{1}{r}\int_V \rho(r')d\tau' + \frac{1}{r^2}\int_V \rho(r')r'\cos\theta d\tau' + \frac{1}{r^3}\int_V \rho(r')r'^2\left(\frac{3}{2}\cos^2\theta - \frac{1}{2}\right)d\tau' + \cdots \tag{1}$$

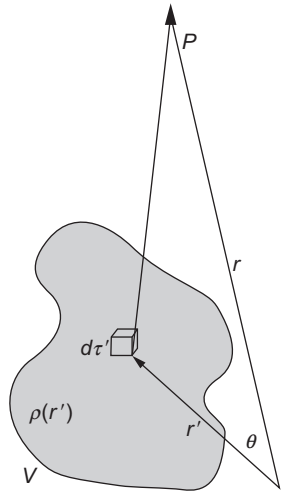

FIG. 1 Definition of the quantities, used in Eq. (1).

with the charge density ρ, cf. Fig. 1. The first term in Eq. (1) represents monopole, i.e., a net charge:

$$V_{Monpole}(r) = \frac{1}{r}\int_V \rho(r')d\tau' = \frac{q}{r} \tag{2}$$

The second term is the quantity we deal here with, the dipole moment:

$$V_{Dipole}(r) = \frac{1}{r^2}\int_V \rho(r')r'\cos\theta d\tau' = \frac{\hat{r}}{r^2}p \tag{3}$$

where p is the dipole moment[3], which for point charges is defined as:

$$p = \sum_{i=1}^{n} q_i r_i' \tag{4}$$

Higher order terms can be constructed from the lower multipole components. A quadrupole moment is constructed from two dipoles, of which one is inverted, an octopole from two inverted quadrupoles, etc.

The dipole of a molecule is characterized by its size and direction, i.e., is a vector quantity. The permanent dipole moment of a molecule is a measure for the charge separation due to a nonuniform distribution of the positive and negative charges. Such nonuniform charge distributions occur for molecules

3. The electric dipole moments have the dimensions of charge times length and the original unit of the dipole moment is the Debye (D). The conversion factor of Debye into SI unit Coulomb meter is 1 D = $3.333 \cdot 10^{-30}$ C m. In units of the elementary charge e 1 Debye is the charge of 0.2082 e in a distance of 1 Å.

without inversion symmetry. As example of nonvanishing dipole moments might serve the case of *cis*-1,2-dichloroethane, while the centrosymmetric *trans*-1,2-dichloroethane lacks a permanent dipole moment in spite of the different electronegativities of the carbon, hydrogen, and chlorine atoms. Each electronic state has a different electron density distribution and therefore different electric dipole moments.

The expectation value of the permanent dipole moment in the electronic ground state of a molecule is defined as:

$$\langle \mu \rangle_g = \int \Psi_g^* \hat{\mu} \Psi_g d\tau \tag{5}$$

The respective expectation value for the electronically excited state is accordingly:

$$\langle \mu \rangle_e = \int \Psi_e^* \hat{\mu} \Psi_e d\tau \tag{6}$$

The energy of interaction of such a (permanent) dipole moment with the electric field $\mathcal{E}$ is given by:

$$E = -\langle \mu \rangle \cdot \mathcal{E} \tag{7}$$

To describe the interaction energy for a light driven transition between two states the transition dipole, rather than the dipole moment is used:

$$\langle \mu \rangle_T = \int \Psi_e^* \hat{\mu} \Psi_g d\tau \tag{8}$$

The transition moment $\langle \mu \rangle_T$ for the transition between a ground (g) and excited (e) state depends on the phase factors associated with the wavefunctions of the two states connected by the transition. It defines both the polarization of a transition through the direction of the vector as well as the strength of the transition through the square of the magnitude of $\langle \mu \rangle_T$.

3 THE STARK EFFECT

The Stark effect describes the shifting and splitting of rotational or rovibrational lines due to the interaction with an external electric field. The Stark effect was discovered in 1913 independently by Stark [9] and Lo Surdo [41]. It is the electric analog to the magnetic Zeeman effect [42, 43].

The theory of the interaction of a static electric field with the dipole moments of diatomic molecules goes back to the early times of molecular quantum mechanics [44, 45]. We will start with a description of the Stark effect for rotating linear and symmetric tops, since for these analytical expressions are available for calculation of the Stark energies. The more general case of asymmetric rotor, which will be solved numerically is given afterwards.

3.1 First Order Stark Effect

The effect of an external electric field $\mathcal{E}$ on the energies of a rotating symmetric top molecule can be obtained from the first order correction to the energy, using standard perturbation theory. For the perturbation of the rigid rotor Hamiltonian H, one obtains:

$$H_{Stark} = \sum_{i,\alpha} -\mathcal{E}_i S_{i\alpha}^{-1} \mu_\alpha \tag{9}$$

with the electric field $-\mathcal{E}_i$ along the space fixed coordinates i, the components of the dipole moment μ along the molecule fixed inertial axes α, and the direction cosine matrix $S_{i\alpha}^{-1}$ [46] to transform space fixed dipole moments into molecule fixed components μ_α. The electric field is chosen along the z axis and for a symmetric top the dipole moment has only components along the symmetry axes. The first order correction is then given by taking the matrix elements of H_{Stark} over the unperturbed wavefunctions in the J, K, M basis:

$$H_{Stark} = -\mathcal{E}_z \mu_\alpha \left\langle JKM \middle| S_{z\alpha}^{-1} \middle| JKM \right\rangle \tag{10}$$

The symmetry axis of a symmetric top is the a axis in the prolate case ($B = C$) or the c axis for an oblate rotor ($A = B$). Evaluating Eq. (10) for the μ component along the symmetry axis, we find as first order corrected energy $E_{Stark}^{(1)}$:

$$E_{Stark}^{(1)} = -\mathcal{E}\mu \frac{KM}{J(J+1)} \tag{11}$$

From Eq. (11) it is immediately obvious, that linear rotors (K always zero) and the $K = 0$ stack of symmetric rotors do not show a first order Stark effect. The components of Stark Hamiltonian along all three inertial axes for an asymmetric rotor will be given in the following.

3.2 Second Order Stark Effect

The energy, corrected to second order is given by:

$$E_{Stark}^{(2)} = \frac{\mu^2 \mathcal{E}^2}{2B} \left[\frac{(J^2 - K^2)(J^2 - M^2)}{J^3(2J-1)(2J+1)} - \frac{[(J+1)^2 - K^2][(J+1)^2 - M^2]}{(J+1)^3(2J+1)(2J+3)} \right] \tag{12}$$

Linear rotors and the $K = 0$ stack of symmetric rotors do not show a first order Stark effect, but the lowest perturbation order is of second order.

While for the first order Stark effect, the M degeneracy is lifted, and each level is split into $2J + 1$ components, the square of M in Eq. (12) causes the degeneracy to be only $J + 1$.

4 HAMILTONIAN FOR THE EVALUATION OF ROVIBRONIC STARK SPECTRA

In what follows we will shortly resume the important details about the molecular Hamiltonian used for the calculation of rovibronic Stark spectra.

4.1 The Rigid Rotor Hamiltonian for Asymmetric Tops

The Hamiltonian for a rigid rotating molecule in terms of the rotational constants, which are related to the moments of inertia with respect to the main inertial axes is given by [47]:

$$H_r = AJ_a^2 + BJ_b^2 + CJ_c^2. \tag{13}$$

Here $J_g (g = a, b, c)$ are the components of the body fixed angular momentum operator, A, B, and C are the three rotational constants. One set of rotational constants is needed for the simulation of microwave spectra, while for rovibrational or rovibronic spectra a second set of rotational constants for the (vibrationally or electronically) excited state are necessary. Using representation I^r for the identification of the main inertial axes a, b, c to the molecule fixed coordinate system x, y, z one obtains the matrix elements in the basis of symmetric rotor wavefunctions $\langle J,K,M|$:

$$\langle J,K,M|H_r|J,K,M\rangle = \frac{1}{2}(B+C)\left(J(J+1)-K^2\right)+AK^2 \tag{14}$$

$$\begin{aligned}\langle J,K,M|H_r|J,K\pm 2,M\rangle = &\frac{1}{4}(B-C)\sqrt{J(J+1)-K(K\pm 1)}\\ &\times\sqrt{J(J+1)-(K\pm 1)(K\pm 2)}\end{aligned} \tag{15}$$

4.2 The Centrifugal Distortion Hamiltonian for Asymmetric Tops

Quartic and sextic centrifugal distortion constants may be included if necessary through the model of a distortable rotor in Watson's A-reduced form [48]:

$$\begin{aligned}H_{dist} = &-\Delta_J J^4 - \Delta_{JK} J^2 J_a^2 - \Delta_K J_a^4\\ &-2\delta_J J^2\left(J_b^2 - J_c^2\right) - \delta_K\left[J_a^2\left(J_b^2 - J_c^2\right) + \left(J_b^2 - J_c^2\right)J_a^2\right]\\ &+H_J J^6 + H_{JK} J^4 J_a^2 + H_{KJ} J^2 J_a^4 + H_K J_a^6\\ &+2h_J J^4\left(J_b^2 - J_c^2\right) + h_{JK} J^2\left[J_a^2\left(J_b^2 - J_c^2\right) + \left(J_b^2 - J_c^2\right)J_a^2\right]\\ &+h_K\left[J_a^4\left(J_b^2 - J_c^2\right) + \left(J_b^2 - J_c^2\right)J_a^4\right]\end{aligned} \tag{16}$$

Hence the total rotational Hamiltonian becomes

$$H_R = H_r + H_{dist} \tag{17}$$

If quartic centrifugal constants are sufficient for description of the spectra, five additional parameters, Δ_J, Δ_{JK}, Δ_K, δ_J, and δ_K in Watson's A-reduction [48] must be considered for each electronic state. For very weakly bound complexes, it might become necessary to employ also sextic centrifugal distortion constants what would add another seven parameters for each electronic state. The matrix elements of the distortable rotor have the same form as the matrix elements of the rigid rotor:

$$\begin{aligned}\langle J,K,M|H_r|J,K,M\rangle = &\frac{1}{2}(B+C)\left(J(J+1)-K^2\right)+AK^2 \\ &-\Delta_J J^2(J+1)^2-\Delta_{JK}J(J+1)K^2-\Delta_K K^4\end{aligned} \tag{18}$$

$$\begin{aligned}\langle J,K,M|H_r|J,K\pm 2,M\rangle = &\frac{1}{4}(B-C)-\delta_J J(J+1) \\ &-\frac{1}{2}\delta_K\left[(K\pm 2)^2+K^2\right]\times\sqrt{J(J+1)-K(K\pm 1)} \\ &\sqrt{J(J+1)-(K\pm 1)(K\pm 2)}\end{aligned} \tag{19}$$

4.3 The Stark Hamiltonian for Asymmetric Tops

In the presence of a dc electric field $\mathcal{E}$ additional terms arise from the Stark effect. The first order Stark Hamiltonian can be written as:

$$H_{Stark} = \sum_{i,\alpha} -\mathcal{E}_i S_{i\alpha}^{-1}\mu_\alpha \tag{20}$$

With the electric field direction arbitrarily defined in z-direction, this Hamiltonian can be factorized into the three projections of the dipole moment μ onto the main inertial axes a, b, and c. For the a component one obtains the matrix elements [49]:

$$\langle J,K,M|H^a_{Stark}|J,K,M\rangle = -\mu_a\mathcal{E}\frac{MK}{J(J+1)} \tag{21}$$

$$\langle J+1,K,M|H^a_{Stark}|J,K,M\rangle = -\mu_a\mathcal{E}\frac{\sqrt{(J+1)^2-K^2}\sqrt{(J+1)^2-M^2}}{(J+1)\sqrt{(2J+1)(2J+3)}} \tag{22}$$

For the b-component [49]:

$$\langle J,K+1,M|H^b_{Stark}|J,K,M\rangle = -\mu_b\mathcal{E}\frac{M\sqrt{(J-K)(J+K+1)}}{2J(J+1)} \tag{23}$$

$$\langle J+1, K\pm 1, M|H^{b}_{Stark}|J,K,M\rangle = \mu_b \mathcal{E}\frac{\sqrt{(J\pm K+1)(J\pm K+2)}\sqrt{(J+1)^2-M^2}}{2(J+1)\sqrt{(2J+1)(2J+3)}} \tag{24}$$

and for c [49]:

$$\langle J, K+1, M|H^{c}_{Stark}|J,K,M\rangle = i\mu_c \mathcal{E}\frac{M\sqrt{(J-K)(J+K+1)}}{2J(J+1)} \tag{25}$$

$$\langle J+1, K\pm 1, M|H^{c}_{Stark}|J,K,M\rangle = -i\mu_c \mathcal{E}\frac{\sqrt{(J\pm K+1)(J\pm K+2)}\sqrt{(J+1)^2-M^2}}{2(J+1)\sqrt{(2J+1)(2J+3)}} \tag{26}$$

While the rigid rotor and distortable rotor Hamiltonians without electric field are off-diagonal only in K, connecting matrix elements $K, K\pm 2$, but diagonal in J, i.e., individual Hamilton matrices can be set up for each value of J (cf. Eqs. 14, 15, 18, 19), the Stark Hamiltonian also connects levels $J, J\pm 1$ what leads to large matrix sizes on one hand side and leaves the projection of the total angular momentum along the external field, M as only good quantum number. The projection onto the external Z-axis M can take integral values between $-J$ and $+J$. The Stark Hamiltonian is blockdiagonal in M. The rigid rotor Hamiltonian (Eq. 17) is blockdiagonal in J (each block having the dimension of $2J+1$) and can be factorized into four submatrices using the symmetry elements of the Four group [47]. An external electric field mixes these blocks. If one or more dipole components are zero, the Hamiltonian can still partially be factorized. The symmetry properties for the different cases have been reported by Chang et al. [50]. For the most general case, in which the molecule has dipole moments components along all three inertial axes, the Four group symmetry is lifted and no further factorization of the Hamiltonian can be performed.

5 SELECTION RULES

The selection rules for transition between Stark shifted energy levels of rigid rotors depend on the relative field geometries of the static electric field and the oscillating field of the electromagnetic wave. Since M is the only remaining good quantum number, the selection rules differ from the normal asymmetric rotor selection rules. They only depend on the projection of the angular momentum on the external Z-axis, which is defined by the electric field M, and on the orientation of the electric field to the plane of the electromagnetic wave. Since M is the projection of J onto the external z-axis, than transitions induced by an electromagnetic field, which is polarized in z-direction can only occur if the change in M equals zero. In fact, an electric field in z-direction cannot exert a torque about the z axis.

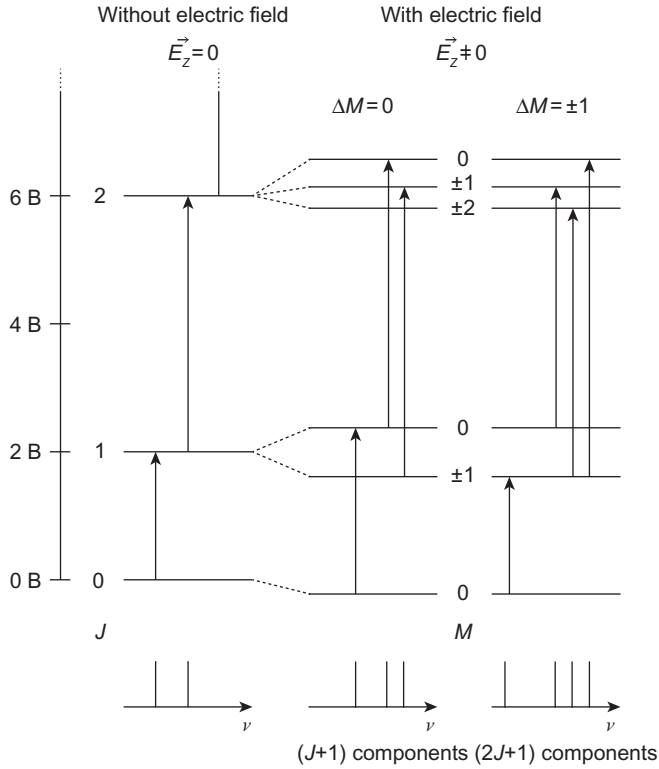

FIG. 2 Transitions between the $J = 0$, $J = 1$, and $J = 2$ levels of a linear rotor according to zero-field conditions (*left*) and following $\Delta M = 0$ (*middle*), and $\Delta M = \pm 1$ (*right*).

Two cases must be distinguished:

- For the light vector being parallel to the electric field vector: $\Delta M = 0$
- For the light vector being perpendicular to the electric field vector: $\Delta M = \pm 1$

In Fig. 2 the Stark splitting for the $J = 1 \rightarrow 2$ of a linear rotor is shown and the resulting transitions due to the different selection rules in M.

In classical waveguide microwave spectroscopy, the electric field is always parallel to the polarization plane of the MW radiation and $\Delta M = 0$ selection rules hold. In molecular beam electric resonance $\Delta M = \pm 1$ transitions are allowed [51]. In optical spectroscopy a rotation of the plane of the light polarization is possible. Hence, both type of transitions can be observed with one experimental set-up, when the polarization plane is rotated. This fact will be exploited later, in order to allow for a more accurate determination of the excited state dipole moment.

6 THEORY OF EVOLUTIONARY ALGORITHMS FOR THE ASSIGNMENT AND FIT OF SPECTRA

Increasing resolution and/or sensitivity of spectroscopic methods leads to an increasing complexity of the spectra, since the more spectroscopic details can be resolved, the greater is the number of parameters needed to describe the spectra. The classical evaluation of the parameters that are needed to describe high-resolution spectra was based for decades on pattern recognition by the eye, i.e., relied on the experience of the user. Over the years, a number of automated methods and computer programs have been developed that greatly helped the analysis of such complex spectra.

The earliest attempt for an automated assignment of rotationally resolved infrared and electronic spectra is the method invented by Loomis and Wood [52]. The lines in a rotational subband of a symmetric top or linear molecule have a roughly constant spacing. The spectra are cut into segments of equal length. If the length of the segments matches the spacing, then the subband will appear as a vertical succession of points. This graphical representation was described in the original paper of Loomis and Wood on the rotational structure of the electronic ^{1}P–^{1}S band of the sodium dimer: "*The other bands in the region studied are so complicated by overlapping lines that the series cannot be followed by inspection. They can, however, be followed in a table of computed line frequencies with estimated intensities, and it is quite evident that there are just three branches starting from near the head of each band.*" This method only gained wider applicability to the spectra of asymmetric rotors after microcomputers became available [53–56].

Interactive Loomis-Wood assignment programs allow assignment and regression of lines in a subband via a Loomis-Wood diagram. Not only do these programs help assign spectra, but they are also a convenient means of bookkeeping the assignments of spectra with a large number of lines. Loomis-Wood programs are particularly useful for the analysis of congested spectra of symmetric tops, slightly asymmetric tops, and linear molecules. Neese [57] has developed an interactive Loomis-Wood assignment package[4], which has been written for IGOR Pro, a program for the analysis and display of numeric data. A nice example of a recent application of the Loomis-Wood method can be found in the paper of Thompsom et al. [58].

In this frame the computer program *JB95*[5] developed by David F. Plusquellic [59] should be mentioned. This program has been very successful in the graphical assignment (*by eye*) of high resolution rotationally resolved spectra. The program consists of a graphical user interface based on a Windows platform. Dialog boxes provide a user interface for the calibration, linearization,

4. This package is available at http://fermi.uchicago.edu/oka/freeware.
5. The program and help are available from http://physics.nist.gov/Divisions/Div844/facilities/uvs/jb95userguide.htm.

and manipulation of experimental data and for the generation and optimization of the simulated spectra. Resources are provided for the deconvolution of multiple overlapping rotational bands from different conformations and/or isotopomers of a molecule and for the analysis of molecular spectra when internal rotation, centrifugal distortion, nuclear quadrupole coupling interactions, large amplitude motion, and inertial frame reorientation effects are resolved.

Moruzzi [60] presented an investigation on the feasibility of automated molecular line assignment. Dense rovibrational molecular spectra are normally assigned by strongly interactive computer methods, ranging from commercial spreadsheets to dedicated programs, like Loomis-Wood or Ritz. While a general-purpose, fully automated assignment procedure seems to be out of reach for the near future, he shows that a thorough investigation of the problem can lead to new, more efficient, and less interactive methods, at least in reasonably favorable conditions. Interesting suggestions are provided by some modern *heuristic* problem-solving algorithms, which mimic natural processes. As a first step, he has developed a *transgenic-evolutionary* algorithm, which has successfully assigned artificial spectra of up to almost 3500 lines. He also discusses its performance on an experimental, but *filtered*, methanol spectrum. Possible future improvements and developments of the method, as well as its limits, are discussed.

The group of Neusser [61, 62] has developed the method of correlation automated rotational fitting (CARF), which directly fits the experimental data, without prior assignments. The technique determines the crosscorrelation between the experimental and the theoretical spectrum. The height of the crosscorrelation peak is a measure for the agreement between experiment and theory.

Recently, Western and Billinghurst [63] implemented a tool for automatic line assignment of rotationally resolved spectra in the PGOPHER program[6]. The algorithm calculates the starting positions of the fit transitions from a initial set of constants and iterates possible sets of assignments of the fit transitions to the observed line positions within a user defined confidence interval. No information about line intensities is made use of in this fitting procedure.

In the past decades various computational tools for fast and reliable multiparameter optimizations have been developed. Many of them mimic natural processes, like optimization of the fitness of a population through evolution, or the optimization of (metal) crystal structures through annealing processes. The first methods will be subsumed in the following as evolutionary algorithms (EAs). The use of EAs for solving highly nonlinear and complex processes as the computation of molecular spectra has become widespread. Although they are conceptually simple, their ability in finding the global optimum of a given problem is remarkable.

6. The program is available at http://pgopher.chm.bris.ac.uk.

EAs represent a set of probabilistic search methods, which adapt concepts of natural evolution like fitness, reproduction, mutation, and selection. The basic idea behind all EAs is the encoding of the parameters, which define a given search problem into strings and leaving them to evolve in an artificial environment in order to find an optimum solution.

Three main different EAs have been developed over the years: The genetic algorithm (GA) by Holland [64], the evolutionary strategy (ES) by Rechenberg [65], and the evolutionary programming by Schwevel [66].

6.1 The Genetic Algorithm

A detailed description of the GA used in the automatic assignment and fitting of the spectra described in this chapter can be found in [67–70].

The molecular parameters to be optimized, which are encoded in binary or real type, are represented by a gene. The vector of all genes, which contains the numerical values of all molecular parameters, is called a chromosome. Initially, the values of all parameters are set to random values between lower and upper limits which are chosen by the user. In general these limits are set symmetrically around estimated molecular parameters with a difference that should be large enough to take account of the uncertainties but small enough to narrow the search space sufficiently for a determination of the parameters. For rotationally resolved spectroscopy, estimates are often obtained from ab initio calculations. After each step, the quality of the solutions is checked by comparing the experimental spectrum to the solution. The agreement between both is determined via a crosscorrelation of simulation and experiment and is called the fitness of the solution. A flow-chart of the procedure is shown in Fig. 3.

One optimization cycle, including evaluation of the fitness of all solutions is called a generation. Pairs of chromosomes are selected for reproduction and their information is combined via a crossover process, which interchanges information between two chromosomes. Since crossover only combines information from the parent generations, it basically explores the fitness landscape locally. The value of a small number of bits in the chromosomes is changed randomly by a mutation operator. Mutation can be viewed as a wider exploration of the fitness surface. Mutation prevents the calculation from being trapped in local minima, as is often the case with derivative-based fitting algorithms.

6.2 The Evolutionary Strategy

An ES algorithm starts with one or more parent(s). A parent is a trial solution that corresponds to a set of parameters like in the GA. From this parent an offspring of multiple children (solutions) is generated. The quality of these solutions is checked through its fitness. Depending on the strategy the next parent is

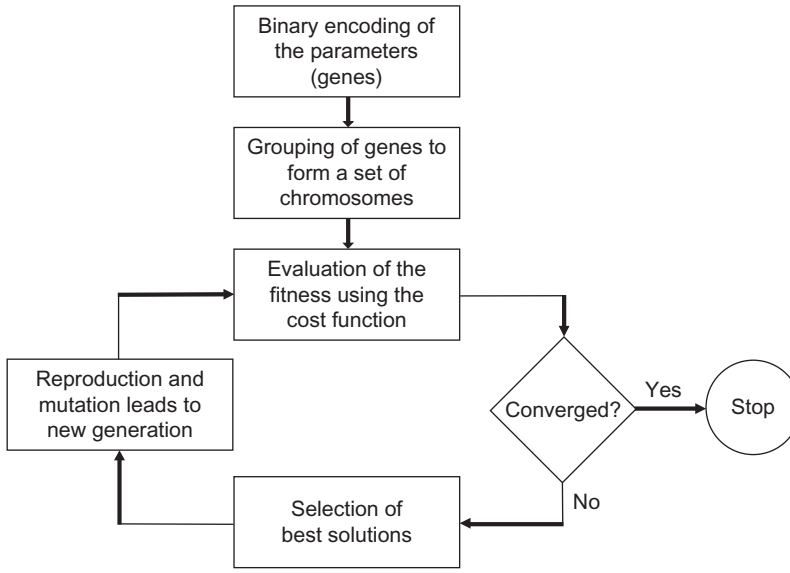

FIG. 3 Schematics of the GA-process.

generated. There are several different strategies for the generation of the offspring as well as the generation of the next parent. For a more detailed description see [65].

The offspring is created from the parent(s) in a mutative step-size control. A drawback of the standard ES is the fact that the mutations of the decision and the strategy parameters, respectively, are subject to independent random processes. If for example, an individual with a large step size undergoes only a very small change in the decision parameters and this small change turns out to yield a high fitness, the large step size will be inherited to the next generation. As a result the fitness in the next mutations may be worsen. This problem is resolved in de-randomized (DR) algorithms which make random mutations in decision and strategy parameters dependent on each other. This idea was implemented for the first as DR1 and soon improved by the concept of accumulated information [71], which is called DR2 and the history of the optimization is recorded and the evolution of the mutation ellipsoid is partially governed by past successful mutations.

A further improvement was achieved by Hansen and Ostermeier [72] with the Covariance Matrix Adaptation Evolution Strategy (CMA-ES). It turns out to be a particularly reliable and highly competitive evolutionary algorithm for local optimization and, surprisingly at first sight, also for global optimization [73]. The CMA-ES does not leave the choice of strategy parameters open to the user—only the population size can be set. Finding good strategy parameters is considered to be part of the algorithm design.

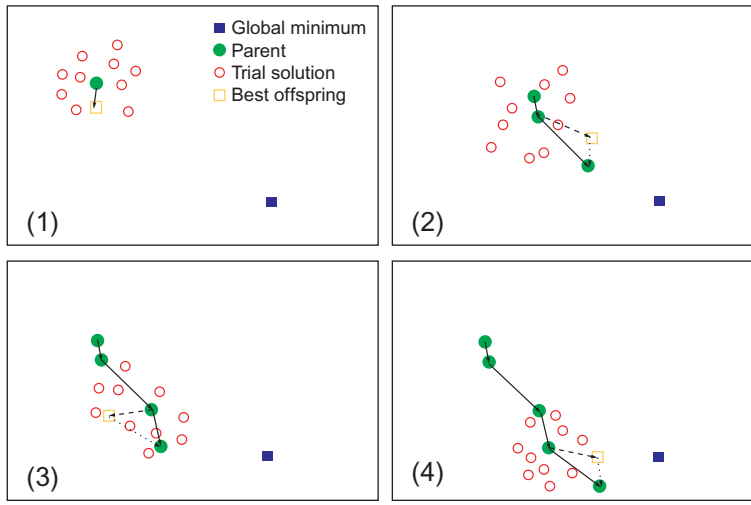

FIG. 4 The first four generations of an evolutionary strategy: (1) An initial population is generated, and the best offspring is used as the next parent. (2) The offspring is spread over a larger area in the second generation due to the relatively large step made in the previous generation. The vector from the parent to the best offspring (*dashed line*) is combined with the (shortened) mutation vector of the last generation (*dotted line*) to generate the new parent (*solid line*). (3) Due to the correlation between the past two mutations the search range has been extended again in the general direction of both mutations while it has been limited in the perpendicular direction. The best offspring is now a local minimum. The memory effect of the evolutionary algorithm, which incorporates past mutation vectors into the calculation of the next parent, helps to overcome the local minimum and the next parent is still closer to the global minimum. (4) The barrier between the local and global minima has been over come, and the optimization is progressing toward the global minimum.

Fig. 4 depicts the first four generations of an ES and demonstrates the effect of the chosen strategy. In general the evolution strategies converge faster and are more rigid than the GA.

6.3 The Fitness Function for the Analysis of Spectra

A proper choice of the fitness function is of vital importance for the success of the EA convergence. It should be calculated sufficiently fast and give a quantitative measure of the goodness of a fit. The value of the fitness function is used to select potential solutions that will survive the current generation, and those that will die out.

Frequently, the deviation of a solution from an objective function is measured via least squares. While for many optimization problems least squares are a reasonable choice, they fail for an evaluation of the agreement of two spectra in the course of the fit. Other objective functions that have been tested for optimization processes are the Manhattan distance as simple absolute distances

of the solution from the aim function [74], Garuti's compatibility index [75], which is based on the inner product between vectors, Saaty's compatibility metric [76], or Pearson correlation coefficient [77].

Meerts et al. [67] have defined a proper fitness function F_{fg} for the use in EA as:

$$F_{fg} = \frac{(\boldsymbol{f}, \boldsymbol{g})}{\|\boldsymbol{f}\|\|\boldsymbol{g}\|} \tag{27}$$

Here $\boldsymbol{f}$ and $\boldsymbol{g}$ are the vector representations of the experimental and calculated spectrum, respectively. The inner product $(\boldsymbol{f}, \boldsymbol{g})$ is defined with the metric $\boldsymbol{W}$ which has the matrix elements $W_{ij} = w(|j-i|) = w(r)$ as:

$$(\boldsymbol{f}, \boldsymbol{g}) = \boldsymbol{f}^T \boldsymbol{W} \boldsymbol{g} \tag{28}$$

and the norm of $\boldsymbol{f}$ as $\|\boldsymbol{f}\| = \sqrt{(\boldsymbol{f}, \boldsymbol{f})}$; similar for $\boldsymbol{g}$. For $w(r)$ a triangle function was used [78] with a width of the base of Δw:

$$w(r) = \begin{cases} 1 - |r| / \left(\frac{1}{2}\Delta w\right) & \text{for } |r| < \frac{1}{2}\Delta \text{ w} \\ 0 & \text{otherwise} \end{cases} \tag{29}$$

One reason for the better performance of this cost function compared to least squares is the fact that molecular rotation spectra show patterns that already appear, when only a subset of the parameters has its correct value. This partial agreement shows up in the crosscorrelation of Eq. (27). Furthermore, the use of a broadening function $w(r)$ results in a smoother error-landscape which allows an easier optimization, since narrow valleys on the cost surface are broadened, allowing the algorithm to converge more smoothly to the correct values. It should be mentioned that the use of the broadening function improves the performance of the GA greatly, but is not necessary for the convergence of the ES.

7 EXPERIMENTAL SET-UP

7.1 Rotationally Resolved Electronic Stark Spectroscopy

The experimental set-up for rotationally resolved electronic spectroscopy in molecular beams has been described in great detail many times [70, 79–81]. Therefore, we will give only a very short resume of the method and concentrate on the changes that have to be made in order to determine excited state dipole moments. A laser system is needed that emits in the visible (400–750 nm) and/or in the UV (400–250 nm) range, with a resolution of about 1 MHz or better. At a typical wavelength of 300 nm a bandwidth of 1 MHz is equivalent to a resolution of 1 in 10^9. The problem of Doppler broadening in electronic spectroscopy is severe, since Doppler broadening is proportional to the excitation frequency. Thus, the Doppler broadening in the than 10^6 times larger than in the microwave region. The application of seeded molecular beams [82, 83],

which are crossed at right angles with angles with the laser considerably reduces the Doppler broadening. A further reduction of the Doppler width can be achieved by confining the molecular beam to a small angular range about the beam axis using one or more skimmers. By means of this geometric limitation of the molecular beam in the direction of the laser beam a reduction of the velocity distribution in a thermal ensemble by a factor of 200 can be achieved. Thus, the Doppler width which in a thermal ensemble of Argon at 373 K at a central wavelength of 300 nm amounts to about 2 GHz can be reduced to 10 MHz by pure geometric skimming. Fig. 5 shows a typical molecular beam setup used for rotationally resolved electronic spectroscopy. The molecular beam, which is formed by expansion of the probe (a), seeded in Argon through the nozzle (b) is skimmed twice (c,d) for a maximum reduction of the Doppler width. The beam is crossed at right angles with the laser light and the fluorescence is collected at right angles though imaging optics (e) onto a photomultiplier (f). The molecular beam position can be controlled by means of a quadrupole mass spectrometer (g).

An electric field has to be applied in order to observe the Stark effect in the interaction region of the laser beam with the molecular beam (2). In contrast to Stark spectroscopy on microwave spectroscopy, the signal (fluorescence light) is observed perpendicular to the applied field. Thus, at least the electrode in

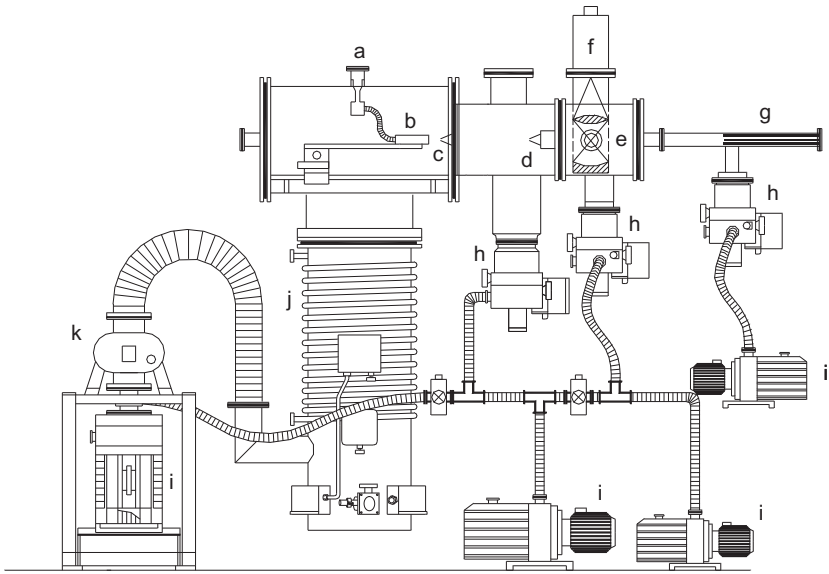

FIG. 5 Molecular beam machine used for the experiments described in this chapter. (a) probe container; (b) nozzle; (c,d) beam skimmers; (e) imaging optics; (f) photomultiplier; (g) quadrupole mass spectrometer; (h) turbo-molecular pumps; (i) rotatory pumps; (j) oil diffusion pump; (k) roots blower pump.

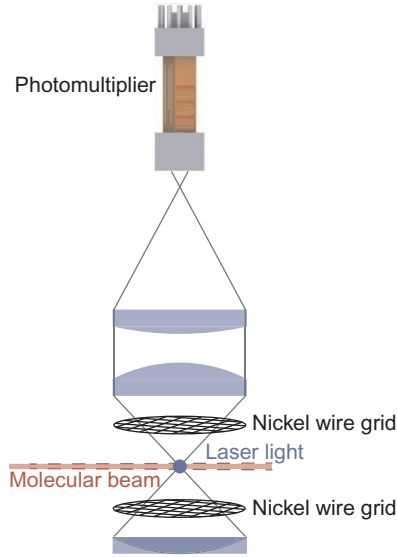

FIG. 6 The imaging optics with the Stark plates mounted. The distance of the Stark plates has to be adjusted to maximize the field strength and to minimize the stray light. Optimum distances are between 1 and 2 cm.

direction of the photomultiplier (f) has to be transparent for UV light. Fig. 6 shows the modified interaction region using a parallel pair of electro-formed nickel wire mesh (18 mesh per mm, 50 mm diameter) with a transmission of 95% in the UV. These meshes are optimized as transmittive grid electrodes for time-of-flight mass spectrometric applications. Their mutual distance is roughly 23 mm, symmetrically with respect to the laser beam. Since the energy of the Stark shifted lines in the spectra and therefore the dipole moments depend on the electric field strength, i.e., the ratio of voltage and distance U/d, the exact determination of the distance of the plates is crucial for the accurate calculation of the dipole moments.

The voltage applied to the Stark plates is generated by a stabilized high voltage source, which is stable to 1‰. The precision, with which the dipole moment can be determined, therefore depends on the exact knowledge of the plate distance. In order to obtain this distance the electronic Stark spectrum of a substance is measured for which the microwave Stark spectrum and the ground state dipole moments are known to a high accuracy. The plate distance can then be fitted using the combination differences of transitions in the UV spectrum that match the tabulated MW lines. The best primary standard for ground state dipole moments of isolated molecules is OCS [84]. Since this molecule does not fluoresce a secondary standard, which has been calibrated to the OCS microwave spectrum can be used. The condition that the molecule should have a high dipole moment and fluoresce strongly limits the search to a few systems.

The best standard is the benzonitrile spectrum, for which MW spectrum and dipole moments have been reported [85].

A few words about the homogeneity of the applied electric field. We follow Ref. [86, equations (19) + (20)]:

$$E(0,0,z) = E(0,0,0)R^3/(z^2+R^2)^{3/2} \tag{30}$$

With $4/3\pi^3 = 1$ mm^3 (at maximum) follows $z = 0.62$ mm and from the radius of the Stark plates $R = 25$ mm we obtain $E(0, 0, 0.62) = 1.0009$. This is a deviation of $9 \cdot 10^{-4}$. Thus, $\Delta E/E_0 \approx 1 \cdot 10^{-3}$. This means the spread in the frequency is $\Delta\nu = 2 \cdot 10^{-3} \cdot \nu$ due to the quadratic Stark effect. Up to Stark shifts of 2000 MHz, the broadening $\Delta\nu$ is less than 4 MHz, which is considerably smaller than the line-widths in the UV, hence effects due to inhomogeneity of the field are negligible.

The polarization plane of the incoming laser beam can be rotated by 90° inside the vacuum chamber by means of an achromatic $\lambda/2$ plate (Bernhard Halle 240–380 nm). The $\lambda/2$ plate can be pushed in or pulled out from the beam-way using a linear motion vacuum feedthrough. The experimental set-up is shown in Fig. 7.

With the $\lambda/2$ plate inside the beamway, the polarization plane of the incoming laser beam is rotated from vertical to horizontal orientation. The $\lambda/2$ plate is placed inside the vacuum chamber, since the entrance windows of the vacuum chamber are mounted under Brewster's angle in order to improve the light transmission through the window and minimize the stray light, that might interfere inside the chamber with the fluorescence light. Thus, within a second it is possible the change the relative orientation of EM wave and electric field, to switch between different selection rules for the observed spectra. Fig. 8 shows the different Stark spectra of 5-methoxyindole for parallel ($\Delta M = 0$) and the black trace to perpendicular polarization of the laser beam to the electric field ($\Delta M = \pm 1$).

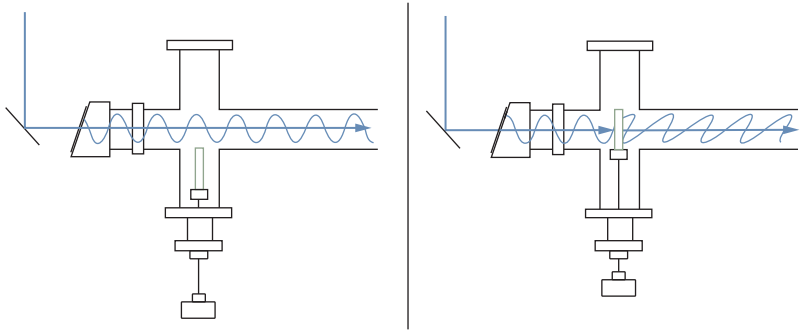

FIG. 7 Coupling of the polarized laser radiation into the molecular beam machine. The shown set-up is perpendicular to (e) in Fig. 6.

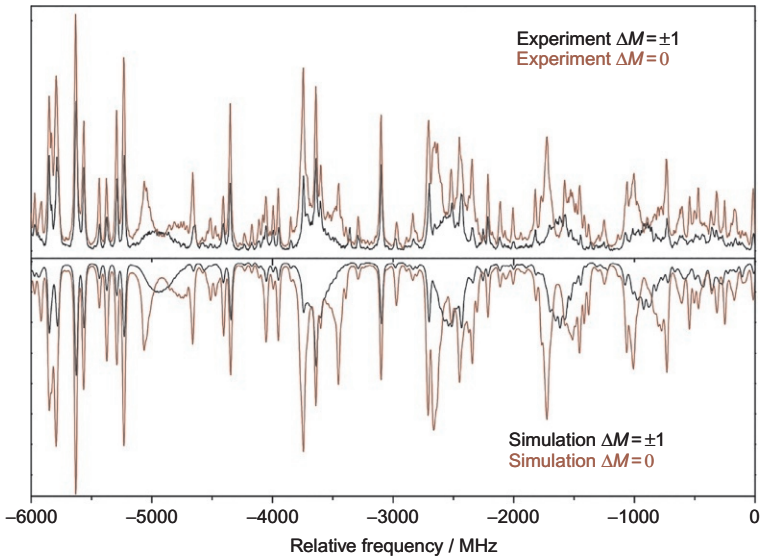

FIG. 8 Experimental Stark spectra of the electronic origin of the anticonformer of 5MOI at electric field strengths of 397.19 V/cm. The *red trace* (dark gray in print versions) belongs to parallel ($\Delta M = 0$) and the *black trace* to perpendicular polarization of the laser beam to the electric field ($\Delta M = \pm 1$). The lower half of the figure shows the simulated spectra as they are analyzed with the CMA-ES algorithm.

Using the evolutionary strategies, described in the last section, both spectra with parallel ($\Delta M = 0$) and perpendicular polarization of the laser beam ($\Delta M = \pm 1$) could be fitted simultaneously, improving the accuracy of the dipole moments and reducing the correlations between the parameters [36].

7.2 Excited State Dipole Moments From Experiments in the Time Domain

Apart from the spectroscopic techniques discussed earlier, a time domain approach to excited state dipole moments in the gas phase is used in coherent beat techniques with a Stark field, pioneered in the groups of Sodeik [37], Zare [38], Huber [39], and Tanaka [40].

7.2.1 Electric Field Induced Quantum Beats

Brieger et al. [37] measured the excited state dipole moment of ^{7}LiH using electric field induced quantum beats in the exponential decay after pulsed laser excitation of a single rotational $R(0)$ transition of ^{7}LiH. This method has several advantages over frequency resolved Stark techniques. Corrections due to laser power or rf power, and scanning of the electric field and radio frequency, are not

necessary and the quantum beat signals are easy to evaluate with high accuracy [37]. Ohta and Tanaka [40] determined the excited state dipole moment of pyrimidine to be 0.58 D from Stark quantum beats of pyrimidine vapor observed after excitation at the $R(0)$ and $R(1)$ rotational lines of the origin band belonging to the $S_1 \leftarrow S_0$ transition. The excited state dipole moment is thus considerably smaller than the ground state dipole moment (2.334 Debye), in line with an interpretation of the transition as being due to an $n\pi^*$.

7.2.2 Rotational Coherence Spectroscopy

Another complementary method for the determination of molecular structures in different electronic states exists, which was established by Felker and co-workers is called rotational coherence spectroscopy (RCS) [87], which was in the last few years considerably improved by Riehn [88] and Leutwyler [89, 90].

While the rotational resolution in the frequency domain experiments, is achieved by limiting the spectral band width of the exciting light source, RCS measures the time which a molecule needs for rotation per radian. For large molecules, these times are at the order of a few picoseconds. Thus, to measure the rotational recurrences of large molecules, exciting laser pulses with picosecond or even subpicosecond duration are necessary. In principle it should be possible to perform RCS measurements in an electric field, which should then show altered recurrences of the coherently excited molecules. Fourier transform of these spectra should then yield the dipole moments of the two states. To our knowledge, these experiments have not been performed yet.

8 EXCITED STATE DIPOLE MOMENTS FROM ROTATIONALLY RESOLVED STARK SPECTROSCOPY

In the following we will give a survey of dipole moments of excited states, which have been determined from rotationally resolved Stark spectroscopy in the gas phase, see Table 1. After a short overview on the systems studied until now, we will concentrate on several systems, which show interesting physical and/or chemical properties.

The groups of Klemperer and later Lombardi were the first to implement gas phase electronic Stark spectroscopy after excitation of the sample in a static gas cell with a high-pressure mercury-xenon compact arc lamp and photographing the spectrum after dispersion by a 10-m Echelle spectrograph. The first polyatomic asymmetric rotor ever, investigated by Freeman and Klemperer was the $n\pi^*$ 3390 Å system of formaldehyde [34]. A series of compounds of increasing size has been investigated, comprising $n\pi^*$ states of propynal [91], formylfluoride [92], difluoroazirine [93], and the $\pi\pi^*$ states of fluorobenzene [94], chlorobenzene [95], aniline [25], phenol [25], and styrene [96] (Fig. 9).

TABLE 1 Dipole Moments of Molecules in Their Ground (μ'') and Electronically Excited States (μ'), Their Components μ_g on the Main Inertial Axes $g = a, b, c$, the Difference of the Dipole Moment $\Delta\mu = \mu' - \mu''$, the Angle θ Between the Ground and Excited State Dipole Moment Vector, and the Nature of the Electronically Excited State From Electronic Stark Spectroscopy in the Gas Phase

	μ''	μ''_a	μ''_b	μ''_c	μ'	μ'_a	μ'_b	μ'_c	$\Delta\mu$	θ	Nat.	Ref.
4-Aminobenzoic acid	3.3	3.12	1.2	0	4.4	4.21	1.3	0	+1.1	4	$\pi\pi^*$	[104]
2-Aminobenzonitrile	4.1	3.6	1.9	0	4.8	3.4	3.4	0	+0.7	17	$\pi\pi^*$	[105, 106]
3-Aminobenzonitrile	4.9	4.8	1.2	0	6.8	6.8	0	0	+1.9	14	$\pi\pi^*$	[105, 106]
4-Aminobenzonitrile	6.41	6.41	0.0	0	7.20	7.20	0.0	0	+0.81	0	$\pi\pi^*$	[106]
cis-3-Aminophenol	2.3	1.77	1.5	0	3.3	2.94	1.5	0	+1.0	13	$\pi\pi^*(L_a/L_b)$	[103]
trans-3-Aminophenol	0.7	0.57	0.5	0	1.7	1.70	0.1	0	+1.0	38	$\pi\pi^*(L_a/L_b)$	[103]
Aniline	1.13	1.13	0	0	2.80	2.80	0	0	+1.77	0	$\pi\pi^*(L_b)$	[103, 106]
7-Azaindole	1.59	1.45	0.65	0	2.30	2.23	0.55	0	+0.71	10	$\pi\pi^*$	[110, 111]
Benzonitrile	4.48	4.48	0	0	4.57	4.57	0	0	+0.09	0	$\pi\pi^*$	[106]
5-Cyanoindole	7.14	6.96	1.59	0	8.17	8.01	1.62	0	+1.03	1	$\pi\pi^*(L_a)$	[117]
Difluorodiazirine	0	0	0	0	1.5	–	–	–	+1.5	–	$n\pi^*$	[93]
1,3-Dimethoxybenzene	1.19	1.15	0.31	0	1.42	1.25	0.68	0	+0.33	14	$\pi\pi^*(L_b)$	[118]
Fluorobenzene	1.66	1.66	0	0	1.96	1.96	0	0	+0.30	0	$\pi\pi^*(L_b)$	[94]
4-Fluoroindole	3.41	2.62	2.19	0	2.99	2.39	1.8	0	−0.42	13	$\pi\pi^*(L_b)$	[119]
5-Fluoroindole	3.62	3.27	1.56	0	3.32	3.14	1.07	0	−0.30	7	$\pi\pi^*(L_b)$	[117]
6-Fluoroindole	2.51	2.47	0.44	0	3.38	3.31	0.69	0	+0.87	2	$\pi\pi^*(L_b)$	[119]

1-Fluoronaphthalene	1.41	0.62	1.26	0	1.38	0.52	1.28	0	−0.03	4	$\pi\pi^*(L_b)$	[101]
2-Fluoronaphthalene	1.66	1.56	0.58	0	1.54	1.46	0.49	0	−0.12	2	$\pi\pi^*(L_a)$	[102]
Formaldehyde	2.34	2.34	0	0	1.56	1.56	0	0	−0.70	0	$n\pi^*$	[34]
Formylfluoride	2.02	0.60	1.93	0	2.6	1.66	2.0	0	+0.6	22	$n\pi^*$	[92]
anti-5-Hydroxyindole	2.15	2.14	0.18	0	1.54	1.53	0.17	0	−0.61	2	$\pi\pi^*(L_b)$	[117]
Indole	1.96	1.37	1.40	0	1.86	1.56	1.01	0	−0.11	13	$\pi\pi^*(L_b)$	[108]
Indole-H_2O	4.4	4.2	1.2	0	4.0	3.9	0.9	0	−0.4	14	$\pi\pi^*(L_b)$	[108]
Indole-NH_3	4.8	4.69	1.1	0	4.7	4.53	1.1	0	−0.1	0	$\pi\pi^*(L_b)$	[120]
anti-4-Methoxyindole	0.99	0.82	0.56	0	0.27	0	0.27	0	−0.72	55	$\pi\pi^*$	[121]
anti-5-Methoxyindole	1.59	1.53	0.42	0	1.14	0.41	1.06	0	−0.45	53	$\pi\pi^*(L_b)$	[36]
syn-6-Methoxyindole	2.89	0.22	2.88	0	3.46	0.24	3.43	0	+0.57	0	$\pi\pi^*$	[121]
cis-2-Naphthol	1.01	0.34	0.95	0	1.17	0.16	1.16	0	+0.16	12	$\pi\pi^*$	[113]
trans-2-Naphthol	1.36	0.38	1.31	0	1.44	1.03	1.01	0	+0.08	29	$\pi\pi^*$	[122]
cis-2-Naphthol-NH_3	3.89	2.56	2.93	0	4.94	3.76	3.21	0	+1.03	8	$\pi\pi^*$	[113]
cis-2-Naphthol-H_2O	4.00	3.11	2.51	0	4.66	4.09	2.23	0	+0.66	10	$\pi\pi^*$	[122]
Phenol	1.28	0.13	1.27	0	1.30	0.29	1.27	0	+0.02	7	$\pi\pi^*(L_b)$	[103]
N-phenylcarbazole	1.54	0	1.54	0	1.90	0	1.90	0	+0.36	0	$\pi\pi^*$	[116]
2-Phenylindole	2.08	1.66	1.17	0.45	5.0	4.97	−0.7	0.32	+3.92	43	$\pi\pi^*$	[116]
1-Phenylpyrrole	1.56	−1.56	0	0	0.94	0.94	0	0	+2.50	180	$\pi\pi^*(L_a/L_b)$	[115]
Propynal	2.46	2.39	0.6	0	0.7	0.7	0	0	−1.76	14	$n\pi^*$	[91]

Continued

TABLE 1 Dipole Moments of Molecules in Their Ground (μ'') and Electronically Excited States (μ'), Their Components μ_g on the Main Inertial Axes $g = a, b, c$, the Difference of the Dipole Moment $\Delta\mu=\mu'-\mu''$, the Angle θ Between the Ground and Excited State Dipole Moment Vector, and the Nature of the Electronically Excited State From Electronic Stark Spectroscopy in the Gas Phase—cont'd

	μ''	μ''_a	μ''_b	μ''_c	μ'	μ'_a	μ'_b	μ'_c	$\Delta\mu$	θ	Nat.	Ref.
Tryptamine (GPyout)	1.60	0.60	1.33	0.56	1.40	0.10	1.26	0.46	−0.20	20	$\pi\pi^*(L_b)$	[123]
Tryptamine (GPyup)	2.70	0.40	2.53	0.75	2.50	0.10	2.34	0.87	−0.20	7	$\pi\pi^*(L_b)$	[123]
Tryptamine (Antiup)	2.60	0.70	2.38	0.63	2.50	0.30	2.34	0.66	−0.10	28	$\pi\pi^*(L_b)$	[123]
Tryptamine (GPhup)	2.40	0.90	2.06	0.64	2.20	0.50	2.03	0.62	−0.20	9	$\pi\pi^*(L_b)$	[123]

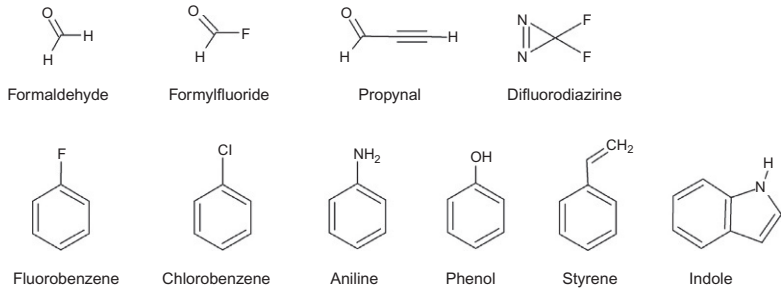

FIG. 9 Overview of molecules that have been investigated with electronic Stark spectroscopy in the Lombardi group.

However, due to the limited resolution in these experiments, very high electric fields had to be applied to observe changes in the spectra.

The next step forward was the use of narrow-band single mode lasers as excitation sources and the use of molecular beam techniques to improve the resolution and accuracy for the structure and dipole moment determinations. The groups of David Pratt at the University of Pittsburgh, Achim Hese at the Technical University of Berlin, and the group of Michael Schmitt at the University of Düsseldorf performed rotationally resolved fluorescence spectroscopy in electric fields in order to determine molecular dipole moments of electronically excited molecules.

Hese investigated cyclic aromatics like benzene [97], pyrazine [98] polycondensed aromatics like anthracene [99], pentacene [100], 1- and 2-fluoronaphthalene [101, 102] (cf. Fig. 10). The centro-symmetric benzene, anthracene, and pentacene molecules posses no permanent dipole moments. Thus, there is no first order Stark effect for these molecules. Upon application of very high field strengths (Hese and co-workers applied up to 250 kV/cm), the external field distorts the electron distribution in the molecule, which results in an induced dipole moment and to the occurrence of spectral shifts, that are quadratically depending on the field strength. The evaluation allows for a

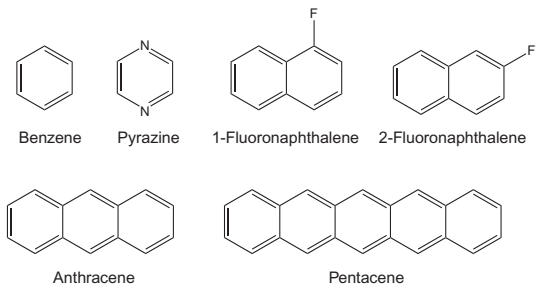

FIG. 10 Overview of molecules that have been investigated with electronic Stark spectroscopy in the Hese group.

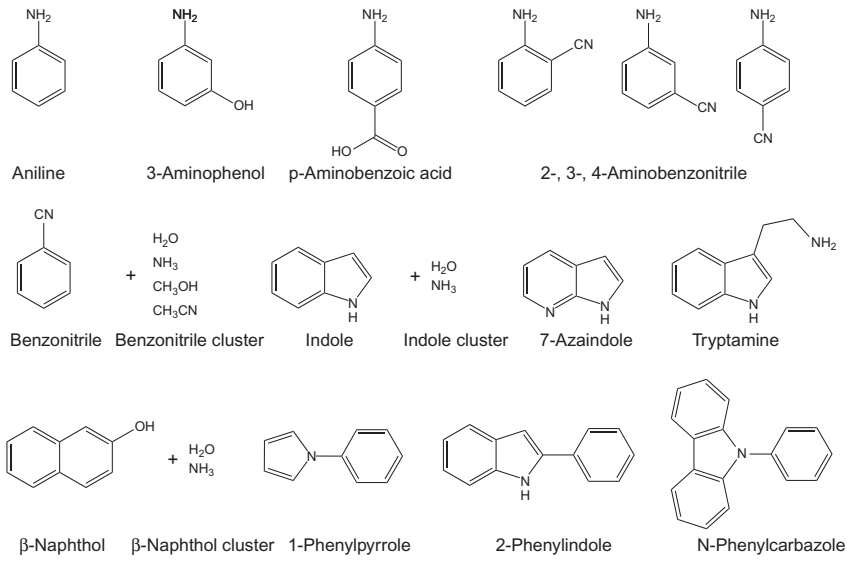

FIG. 11 Overview of molecules that have been investigated with electronic Stark spectroscopy in the Pratt group.

determination of the static polarizabilities of these molecules in both electronic states. In contrast to the vector quantity dipole moment, the polarizabilities are tensors, which measure the flexibility of the electron's density distribution in the molecules.

In the Pratt group different substituted aromatics, like aniline [28]; substituted anilines (3-aminophenol [103], p-aminobenzoic acid [104], 2-, 3-, and 4-aminobenzonitrile [105, 106]); benzonitrile [106]; clusters of benzonitrile with water, ammonia, methanol, and acetonitrile [107]; indole [108]; clusters of indole with water [108] and ammonia [109]; 7-azaindole [110, 111]; and some conformers of tryptamine [112] have been studied. Furthermore, charge-transfer complexes like β-naphthole [113], β-naphthole-ammonia [113], β-naphthole-water [114], and various phenyl substituted heterocyclic aromatics (1-phenylpyrrole [115], 2-phenylindole, and N-phenylcarbazole [116]) were investigated. The structures of the molecules are summarized in Fig. 11.

The group of Schmitt concentrates on excited state dipole moments of substituted indoles. Systems for which dipole moments are reported comprise 4-, 5-, and 6-methoxyindole, 5-cyanoindole, 5-hydroxyindole, and 5-fluoroindole. The structures of the molecules are summarized in Fig. 12.

8.1 The Additivity of Excited State Dipole Moments

A successful concept in chemistry derives the dipole moments of molecules by vectorial addition of individual bond dipole moments. Fig. 13 shows an

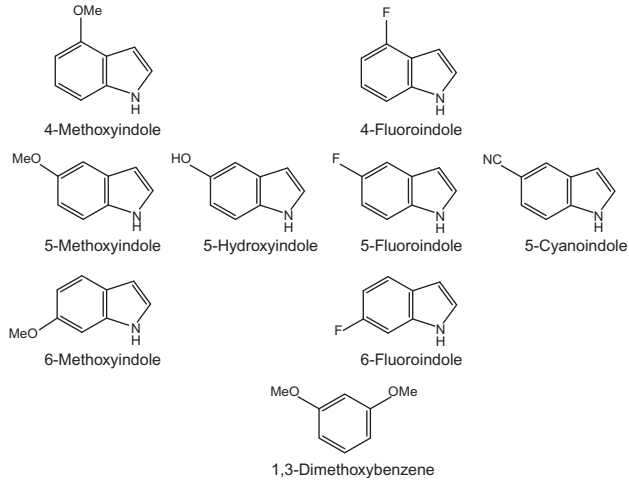

FIG. 12 Overview of molecules that have been investigated with electronic Stark spectroscopy in the Schmitt group.

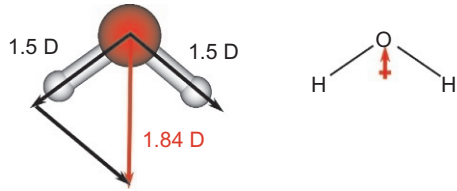

FIG. 13 Vectorial addition of the dipole moment of water from the individual O-H bond dipoles.

example of how the vectorial addition of the two OH bond dipoles sums up of the dipole moment of water. Each O-H bond dipole adds 1.5 Debye to the total dipole moment. With an angle on 104.5° between the bond dipoles, the resulting dipole moment of the water molecule is calculated as $\mu = 2(1.5\,\mathrm{D})\cos(104.5^{\circ}/2) = 1.84\,\mathrm{D}$, cf. Fig. 13. This value is close to the experimentally determined value of 1.8546 D [124]. Using an OH distance in water of 0.96 Å the charges at the oxygen and hydrogen atoms can be calculated to $q(\mathrm{O}) = -0.66e$ and $q(\mathrm{H}) = +0.33e$. Following the convention in chemistry, that for molecules the dipole moment is drawn from the center of the positive to the center of the negative charge (contrary to the definition in physics), a picture like on the right-hand side of Fig. 13 emerges. The small "plus" in the vector of the right-hand side reminds us, that the direction of the dipole moment is from plus to minus (chemical convention). This is maintained throughout the following paragraphs. We also shift the dipole vectors from their center of charge, wherever it is necessary for sake of clarity.

Other textbook examples are the determination of the dipole moments of multiply substituted benzene derivatives, from the known dipole moments of

the individual singly substituted compounds. Fluorobenzene has a ground state dipole moment of 1.66 Debye [94]. The two C-F bonds in 1,2-difluorobenzene form an angle α of 66°. Vectorial addition leads to a dipole moment of $\mu_{12} = 2\cos(\alpha/2) \cdot \mu = 2.71$ Debye. The experimental value, determined from microwave spectroscopy is 2.59 Debye [125]. For the 1,3-disubstituted compound ($\alpha = 120°$) one obtains $\mu_{13} = 1.66$ Debye in fair agreement to the experimental value of 1.51 Debye [125]. The opposing (equal) dipole moments of the C-F bonds in 1,4-difluorobenzene cause a zero dipole moment as observed in the experiment. Deviations from perfect vector additivity in the electronic ground state can be attributed to inductive effects on neighboring bonds, which cancel out in the case of inversion symmetry (Fig. 14).

What happens, if the two substituents are different? Reese et al. [103] studied the two different rotamers of 3-aminophenol, shown in Fig. 15. On the right and left side of Fig. 15 the mono-substituted compounds phenol and aniline, along with the orientations of their dipole moments are shown. The red arrows

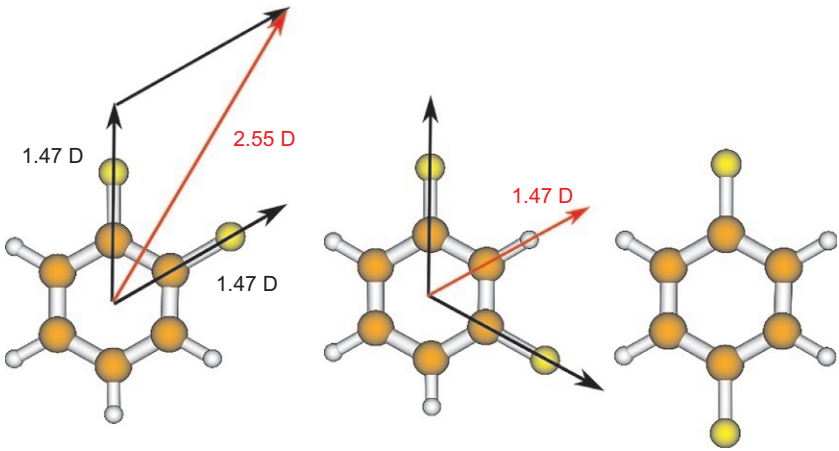

FIG. 14 Vectorial addition of the C-F bond dipoles to yield the dipole moments of o-, m-, and p-difluorobenzene.

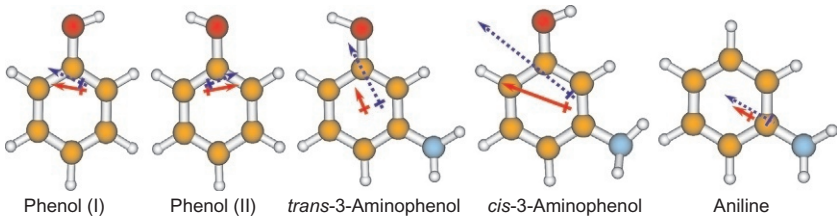

FIG. 15 Dipole moment vectors of *trans*- and *cis*-3-aminophenol and of the monosubstituted constituents phenol and aniline. The *red arrows* (solid lines) gives the dipole moment in the electronic ground state, the *blue arrows* (dotted lines) in the lowest excited singlet state.

(solid lines in the print version) gives the dipole moment in the electronic ground state, the blue arrows (dotted lines in the print version) in the lowest excited singlet state.

The first observation is, that the absolute ground state dipole moments of the *cis* and *trans* rotamers are very different. Vectorial addition immediately shows, that for the *trans* rotamer the dipole moments of phenol and aniline in the ground state just line up to give a larger dipole moment than of any of the constituents. In case of the *cis* rotamer, the aniline and phenol dipole moments have opposing directions and partially cancel out each other. For the ground state dipole moments, vector addition leads to qualitatively correct results, as can be seen for the red vectors in Fig. 15. Taking the vector components of phenol and aniline along the inertial *a* and *b* axes, which are given in Table 1 and rotating them into a common inertial axes system, one obtains a value of 2.35 Debye for the *cis* rotamer and of 0.76 Debye for the *trans* rotamer. Both values are in excellent agreement with the experimentally determined values of 2.3 and 0.7 Debye.

Turning now to the electronically excited state, surprisingly, the vector addition of the S_1 state dipole moments (blue arrows in Fig. 15) fail. Using vector addition of the phenol and aniline S_1 dipole moments, the results are 4.065 and 2.049 Debye for the *cis* and the *trans* rotamer, respectively. Unlike the ground state values, the agreement with the experimental values (3.3 and 1.7 Debye) is not satisfying. However, they agree qualitatively. Still, the dipole moment of the *cis* rotamer is larger than that of the *trans* rotamer, like in the electronic ground state but the deviations are large (0.6 and 0.3 Debye, respectively).

If, in a naive picture, the transition dipole moments of both constituents, aniline and phenol would contribute equally to the excited state of 3-aminophenol, than they should also add up vectorially [103]. This is not observed, as shown in Fig. 16. The reason for the nonadditivity of dipole and transition dipole moments can be found in mixing of the electronically excited states of 3-aminophenol. While the first electronically excited states of both phenol and aniline are pure L_b states[7] (their transition dipole moment intersects the bonds), the lowest two singlet states, L_b and L_a of *trans*- and

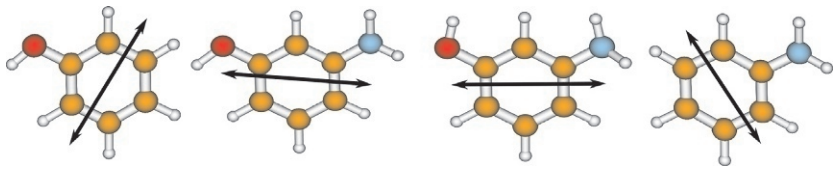

FIG. 16 Transition dipole moment vectors of phenol, *trans*-, *cis*-3-aminophenol, and aniline.

7. The L_a and L_b notation has been introduced by Platt for cata-condensed aromatic hydrocarbons [126]. The labeling scheme has later been extended to indoles by Weber [127]. One has to keep in mind however, that for molecules without twofold rotation axis along the long inertial axis of the molecule, the meaningfulness of this nomenclature is doubtful.

cis-3-aminophenol are mixed. The L_a state has its transition dipole moment running though the atoms, cf. Fig. 16.

For benzene these two states are strictly degenerate and for substituents, that are located on one of the inertial axes (like phenol or aniline) they are quasidegenerate. However, introducing a second substituent in *meta* position to the first rotates the inertial system, leading to an "off-axis" substitution that mixes the excited states. Thus, the excited state dipole moment of 3-aminophenol is attributed to an electronically different excited state (mixed L_a/L_b), than the one of the components (L_b) [103].

The question arises, if this additivity of dipole moments also works for substituted chromophores, in which the chromophore itself has a dipole moment and for electronically excited states of larger molecules with possible interactions of the substituents. A chromophore, which has a permanent dipole in both electronic states by itself is indole. As first system, we will focus on the dipole moments of 5-methoxyindole. Pratt an co-workers determined the dipole moment of indole to be 1.963 Debye in the ground state and 1.856 Debye in the electronically excited S_1 state [108]. The dipole moment vectors are oriented as shown in Fig. 17. The red arrow gives the dipole moment in the electronic ground state, the blue (dotted line in the print version) in the lowest excited singlet state. The excited state dipole vector is rotated by 13° with respect to the ground state vector.

If we now add the methoxy group in 5-position, the dipole moments of the indole chromophore and the methoxy substituent should also add up vectorially. The methoxy group dipole moment is obtained from the incremental values of 0.86 D for the C-O bond dipole and of 1.16 D for the H_3C-O group dipole moment, with an C-O-C angle of 108° [128]. Subtracting the so calculated dipole moment vector of the methoxy group from the experimentally determined *anti*-5MOI ground state dipole moment vector should result in the dipole moment vector of unsubstituted indole. The result is shown in Fig. 18.

The orange difference vector ($\vec{\mu}^{S_0}_{indole} = \vec{\mu}^{S_0}_{5MOI} - \vec{\mu}_{methoxy}$) has indeed the correct direction of the indole dipole moment as shown in Fig. 17. The situation

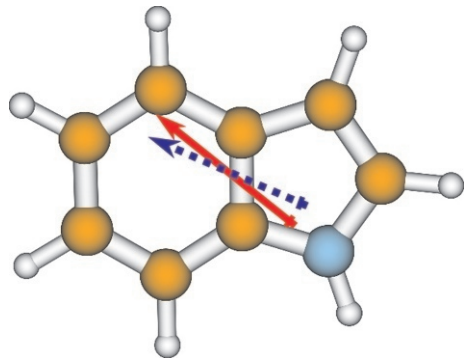

FIG. 17 The dipole moment vectors of indole. The *red arrow* gives the dipole moment in the electronic ground state, the *blue* (dotted line in the print version) in the lowest excited singlet state.

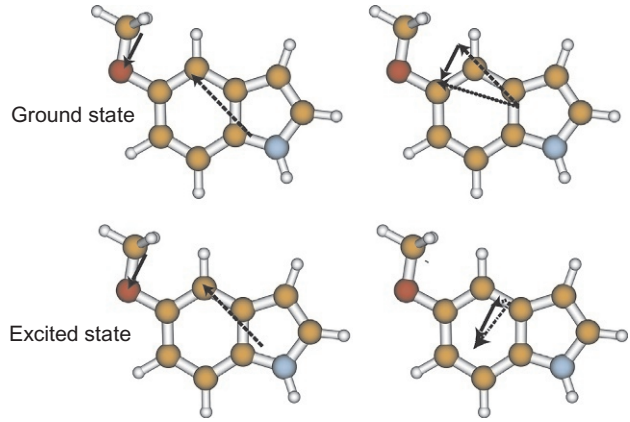

FIG. 18 Left: experimental dipole moment vector of indole (dashed line) and dipole moment increment vector of the OCH_3 group (straight line) for the electronic ground state (upper half) and for the excited state (lower half). Right: vector subtraction of the dipole moment vector of 5-methoxyindole (dotted line) and the dipole moment increment vector of the OCH_3 group (straight line) resulting in the ground state dipole vector of indole (dashed line). For the excited state, the vector subtraction of the dipole moment vector of 5-methoxyindole (dash-dotted line) and the dipole moment increment vector of the OCH_3 group (straight line), results in a vector different from the excited state dipole vector of indole (dashed line).

completely changes for the S_1 state (lower half of Fig. 18) in which vector subtraction of $\vec{\mu}_{5MOI}^{S_1}$ and $\vec{\mu}_{methoxy}$ leads to a vector, which is both in direction and size, completely different from the S_1 state dipole moment vector of indole, shown in Fig. 17.

5-Methoxyindole, indole, and the methoxy group have planar symmetry in the electronic ground state. Thus, the additivity for the dipole moment increments in this state is not surprising. Actually, *off-axis* substitution violates the original condition of Platt (at least C_2-symmetry) for classification as L_a or L_b states. In our case, the energetic difference between L_a and L_b state is much smaller in indole than in 5-methoxyindole. Therefore, it can be argued that for indole the excited states mix to a higher extent. Since the L_a state has a higher dipole moment than the L_b state and a different orientation, the resulting excited state dipole moment depends strongly on the composition of the excited state. This different amount of L_a/L_b mixing in indole and 5-methoxyindole is then the reason for the nonadditivity of the dipole moments in the excited state. Another reason for the nonadditivity of the dipole moments in the excited state might be that 5-methoxyindole shows a considerable participation of charge transfer character in the S_1 state, which is not present in indole. We will come back to this point later.

In many molecules it is possible to determine the direction of the transition dipole moment from the frontier orbitals. However, when strong σ (inductive) effects govern the electron density distribution after excitation, great care has to be taken, not to overstress the fundamental rules, which are based on electron density effects in the π-space in case of the frontier orbitals.

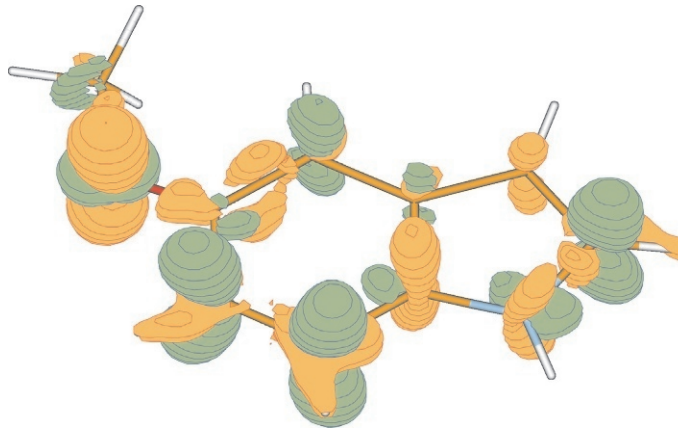

FIG. 19 Electron density difference plot for 5-methoxyindole. *Orange contours* indicate regions with loss of electron density, *green contours* indicate gain of electron density.

Fig. 19 shows a plot of the CC2/cc-pVTZ calculated $S_1 - S_0$ electron density differences. Orange contours indicate regions with loss of electron density, green contours indicate gain of electron density. The charge redistribution upon electronic excitation shows a net charge flow from the pyrrole to the benzene ring as in comparable 5-substituted indoles [129]. The large effect of the methoxy substituent is readily to be seen from Fig. 19. The methoxy π-electron density decreases, because it is shifted into the chromophore upon electronic excitation. Similar shifts of electron density into the aromatic ring upon excitation are observed for phenol [130] and for anisole [131]. On the other hand, the σ-density at the oxygen atom of the methoxy group increases upon electronic excitation. There is an opposite charge density change observed for the σ-electrons compared to the π electrons also for some of the carbon and nitrogen atoms in the indole chromophore. Other atoms show only density changes for the π-electrons. Since the density changes in the σ-electron space are not contained in the picture of frontier orbitals, which all belong to the π-space, the direction of the transition dipole moment in these kind of molecule cannot be determined in a straightforward manner like for smaller or for more symmetric molecules.

A deeper insight into dipole moment additivities requires the comparison of the influence of different substituents at the same position on the excited state dipole moments. In a study on different 5-substituted indoles Wilke et al. [117] performed electronic Stark measurements on 5-fluoroindole, 5-hydroxyindole, 5-cyanoindole, and 5-methoxyindole. As shown earlier, the dipole moment of the indole chromophore and the dipole moment of the methoxy group can be added vectorially to yield the ground state dipole moment of *anti*-5MOI [36], but fails for the excited state. The success of this model depends critically on the mutual influence of the fragment dipole moments. In the following, we will investigate if this behavior is common to substituted indoles and in which cases the model will fail.

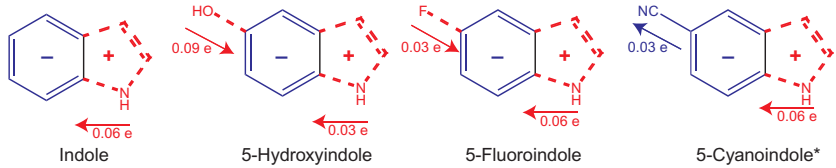

FIG. 20 Charge migrations upon excitation ($\Delta(q_{S_1} - q_{S_0})$) between the pyrrole and phenyl ring of the indole chromophore along with the influence of the respective substituents, calculated with a natural bond orbital analysis at (SCS)*-CC2/cc-pVTZ level of theory. *Blue-colored* (straight lines in the print version) *aromatic rings or substituents* indicate that the respective fragment gain electron density due to the electronic excitation and for *red-colored* (dotted lines in the print version) *dashed aromatic rings or substituents* the electron density decreases.

The hydroxy group, the methoxy group, and the fluorine atom donate electron density to the conjugated π-systems through mesomeric effects (+M), while the mesomerically withdrawing (-M) cyano group decrease the electron density. Additionally, all substituents are exerting an inductive electron withdrawing (-I) effect. In order to get a more quantitative overview, a natural bond orbital (NBO) analysis [132] in the ground and lowest excited state has been performed for all substituted molecules including indole itself. The differences of the natural charges between the ground and the lowest electronically excited state were calculated and are shown in Fig. 20. For the parent molecule indole, an excitation from the ground to the lowest excited state leads to a charge migration of 0.06 electron charges from the pyrrole to the phenyl ring. This value is halved by the addition of a hydroxyl group. Simultaneously, the substituent donates electron density toward the chromophore of about 0.10 electron charges and increases the electron density inside the phenyl ring. The amount of charge which is donated from the substituent upon excitation varies depending on the substituent.

In the case of 5-fluoroindole and 5-cyanoindole the direction of charge migration from the pyrrole to the phenyl ring is the same as in indole. Furthermore, the effect of the substituents on the π-system is significantly smaller than for 5-hydroxyindole and 5-methoxyindole. All substituents with the exception of 5-cyanoindole are donating electron density upon excitation from the ground to the lowest electronically excited state. Thus, we postulate that the additivity-model fails when the flow of electron density from the substituent is opposed to that inside the indole chromophore. This is observed for 5-hydroxyindole, 5-methoxyindole in their S_1-states. When the effect is weak or the substituent supports the natural charge migration inside the bare chromophore, the model also works in the excited state. This is the case for 5-fluoroindole and 5-cyanoindole.

8.2 The Direction of Excited State Dipole Moments

Table 1 gives the dipole moments in ground and electronically excited state along with the angles between the dipole moments, calculated from the ground and excited state components onto the main inertial axes. Most of the molecules

show changes of the dipole orientations larger than 10°. Thus, one of the central approximations in the application of the Lippert-Mataga equation is often violated in real systems. The most extreme cases will be highlighted in the following sections.

8.2.1 1-Phenylpyrrole: Reversal of the Dipole Moment by Electronic Excitation

The determination of dipole moments of the ground state and the lowest electronically excited singlet state of 1-phenylpyrrole using electronic Stark spectroscopy in the group of Pratt showed the surprising result that the dipole moment reverses its direction upon electronic excitation [115]. 1-Phenylpyrrole has a twisted structure in the ground state, with a dihedral angle between the benzene and the pyrrole rings of approximately 20°. In the excited state the inertial defect[8] of the molecule is considerably smaller, showing that 1-phenylpyrrole is more planar in the excited state.

This structural finding already rules out that a TICT state[9] is responsible for the long wavelength shoulder in observed in the fluorescence spectrum in acetonitrile [133].

Stark spectroscopy cannot determine the absolute sign of the dipole moment components[10]. However, the intensities are sensitive to the relative signs of the dipole moments and this results in different Stark patterns. In the present case, this means, that (+/+) and (−/−) orientations give rise to identical spectra, which are different from (+/−) and (−/+) combinations. Fig. 21 shows the result of the dipole moment determination from the electronic Stark spectra. While for

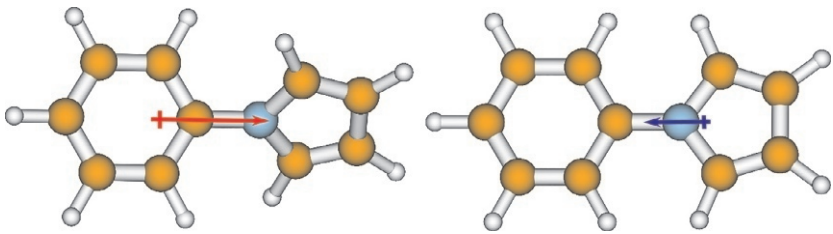

FIG. 21 Dipole moments in the ground state (*left*) and the lowest excited singlet state (*right*) of 1-phenylpyrrole.

8. The inertial defect is a measure for the nonplanarity of a molecule in a given electronic state, and is defined as: $\Delta I = I_C - I_A - I_B$. For a planar molecule it is close to zero.
9. The acronym TICT stands for twisted intramolecular charge transfer. It is quite common for molecules that are composed of an electron donor and an electron acceptor part, which are connected by a single bond. Upon electronic excitation the molecule undergoes a fast charge-transfer, which is accompanied by a twisting of the two parts of the molecule into a perpendicular arrangement. In polar solvents emission from this TICT state has a characteristic strong red-shift.
10. This is due to the fact, that only the projection of J onto the external (Z) axis can be determined.

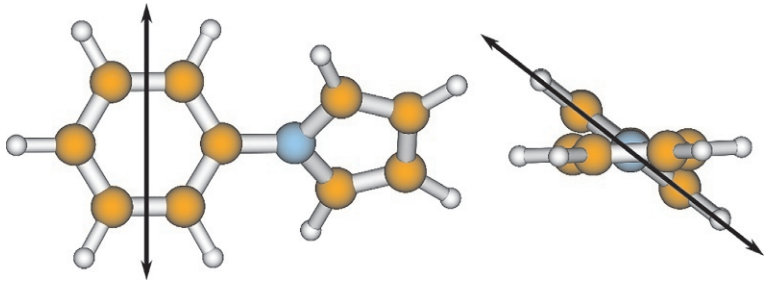

FIG. 22 Two different perspectives of the transition dipole moments orientation in 1-phenylpyrrole. The direction of view in the right figure is from the benzene ring onto the pyrrole ring.

the twisted ground state, a dipole moment of 1.56 Debye is found, which is directed from the positive center of charge at the benzene ring to the pyrrole ring, the dipole moment in the excited state decreases to 0.94 Debye and reverses its orientation. This absolute change of 2.5 Debye is equivalent to a shift of approximately 0.15 electron charges from the pyrrole ring to the benzene ring, whose centers of mass are separated by 3.6 Å [115].

It is probable, that the excited state in this case is not a pure L_b electronic state, but results from a mixed local/charge transfer excitation from vibronic coupling to the higher-lying L_a-state [115, 134]. However, the orientation of the transition dipole moment in 1-phenylpyrrole is located in the plane of the benzene moiety, perpendicular to the long axis of the molecule and twisted by 21°, cf. Fig. 22 as deduced by Thomas et al. [115] from a hybrid character of the zero-field spectrum of 1-phenylpyrrole, consisting of 87.5% *b*-type and 12.5% *c*-type, without any *a*-type character.

Such a localization of the transition moment in the benzene moiety and its orientation, intersecting the bonds of the benzene moiety, point clearly to a pure L_b electronic state.

8.2.2 Methoxyindole: Excited State Dipole Moments of Different Rotamers

The indole chromophore has four possible substitution positions in the benzene moiety and three more in the pyrrolic ring. Electronic properties of the excited states are not only governed by the nature of the substituents, but also strongly by its position.

This has been shown in several studies from our group [36, 119, 121]. For methoxyindole each conformer has two possible orientations of the methoxy group, leading to *syn* and *anti* rotamers, according to the methyl orientation with respect to the pyrrolic N-atom, cf. Fig. 23.

But even this slight geometry change can have a strong influence on the stabilities and further molecular properties of the conformers.

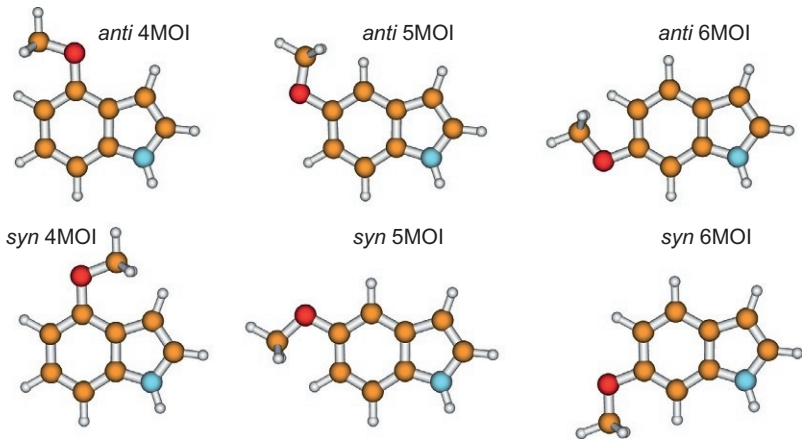

FIG. 23 *Syn*- and *anti*-rotamers of 4-, 5-, and 6-methoxyindole.

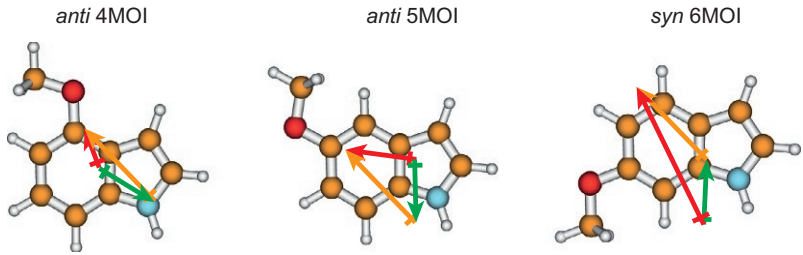

FIG. 24 Vector addition of the indole and the anisole dipole moments and the resulting dipole vectors for *syn*-6-methoxyindole and for *anti*-4-methoxyindole and *anti*-5-methoxyindole.

For the three experimentally observed conformers of methoxyindole, the dipole moments in the ground state can be constructed by vectorial addition of the anisole dipole moment [135] and the indole dipole moment [108]. In all three conformers, the agreement between the vectorially added and the experimental dipole moments is close. The results of the vector additions are shown in Fig. 24.

Surprisingly, not all six possible rotamers are observed in molecular beam experiments but only three of them. For the 4- and 5-methoxyindole conformers, only the *anti* rotamer is observed, while for 6-methoxyindole, the *syn* rotamer is the only one present in the molecular beam spectra. Inspection of the excited state dipole moments of the observed rotamers shows, that the dipole moments of the excited states of the *anti* rotamers decrease by about half of a Debye, while that of the *syn* rotamer increases by approximately the same amount. Even more surprising than the magnitude of the dipole moments are the changes of the orientations of the dipole moments. According to Table 1 the angle between the ground and excited state dipoles is more than 50° for the *anti* rotamers and 0° for the *syn* rotamer.

8.3 State Labeling Using Excited State Dipole Moments

Different electronically excited states have different electron density distributions and therefore differ in magnitude and orientation of their dipole moments. Especially for molecules, which have very close-lying electronically excited states, the determination of dipole moments may help in the classification of the excited state. The emission properties of the aromatic amino acid tryptophan critically depend on the polarity of the local surrounding [136]. The photophysics of the aromatic amino acid tryptophan is governed by their lowest two excited singlet states, which are labeled according to Platt's scheme [126] as L_a and L_b states. They differ in the orientation of the transition dipole moment, which therefore has been used in numerous studies both in gas phase [137–142], as well as in condensed phase [143–145] for an assignment of observed spectral features to a specific excited state. However, there is a strong *caveat*, since only the projection of the transition dipole moment on the main inertial axes can be determined. This leads to an inherent uncertainty, which only can be resolved with further experiments or by comparison to theory. However, while the geometries and static dipoles for each state can be calculated with state of the art quantum chemical calculations, the angle and magnitude of the transition dipole moment has much larger computational uncertainties. Since the L_a state has a much larger permanent dipole moment compared to the L_b state, determination of excited state dipole moments can be utilized for a state labeling in difficult cases.

8.3.1 Cyanoindole

The nitrile group in 5-cyanoindole has a very strong positive mesomeric effect and resulting from that a high dipole moment already in the electronic ground state. The large dipole moment of 5-cyanoindole leads to large spectral Stark shifts, as can be seen in Fig. 25. Already for moderate field strengths of 200 V/cm the spectrum changes completely from the zero-field spectrum [117]. The fit to the $\Delta M = 0$ spectrum in Fig. 25 yields an excited state dipole moment of 8.17 Debye, which is 1.03 Debye larger than in the electronic ground state.

Table 2 collects the properties of the ground and lowest two excited singlet states of 5-cyanoindole, calculated at their respective minimum geometries using spin component scaled approximate coupled cluster singles and doubles model (CC2) employing the resolution-of-the-identity approximation (RI) [146–148]. Given are the main contributions to the excited states, the oscillator strengths f, the transition dipole moment orientations θ with respect to the inertial a-axis, the adiabatic excitation energies ν_0 in cm^{-1}, and the permanent dipole moments μ in Debye. 5-Cyanoindole has a very high dipole moment of 7.1 D already in the electronic ground state, resulting from the push/pull properties of the NH/CN groups. In the S_1 state the dipole moment increases moderately to 8.1 D, while for the S_2 state a large permanent dipole of 10.1 D is calculated. For this state, the permanent dipole moment is oriented

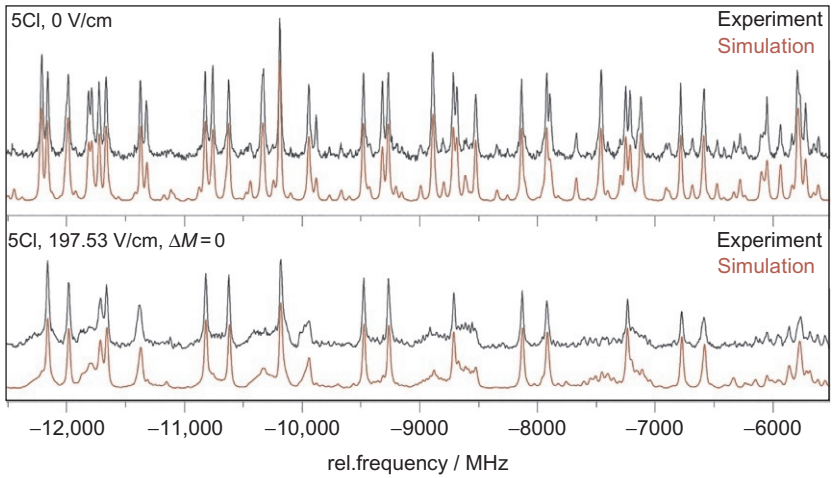

FIG. 25 Zero-field and Stark spectra of 5-cyanoindole in a molecular beam.

TABLE 2 SCS-CC2 Calculated Properties of the Ground and Lowest Two Electronically Excited States of 5-Cyanoindole at Their Respective Minimum Geometries

State	S_0	S_1	S_2
	–	+0.56HOMO → LUMO	0.77HOMO → LUMO
Main	–	−0.51HOMO − 1 → LUMO	+0.44HOMO − 1 → LUMO
Contributions	–	+0.44H − 1 → L + 1	−0.29H → L + 1
	–	+0.42HOMO → LUMO + 1	−0.26HOMO − 2 → LUMO
ν_0/cm^{-1}	–	34,811	37,002
f	–	0.01	0.03
$\theta/°$	–	9.4	65.1
μ/D	7.1	8.1	10.1
$\theta_D/°$	15.8	12.9	3.0

nearly exactly along the inertial a-axis (cf. angle θ_D in Table 2), while the dipole moment of the S_1 state is tilted by 13° with respect to the a-axis and that of the ground state is rotated by 16°.

The adiabatically lowest S_1 state is characterized by $0.56(\text{HOMO} \rightarrow \text{LUMO}) - 0.51(\text{HOMO} - 1 \rightarrow \text{LUMO}) + 0.44(\text{HOMO} - 1 \rightarrow \text{LUMO} + 1) + 0.42(\text{HOMO} \rightarrow \text{LUMO} + 1)$ excitation (cf. Fig. 26). The S_2-state is comprised

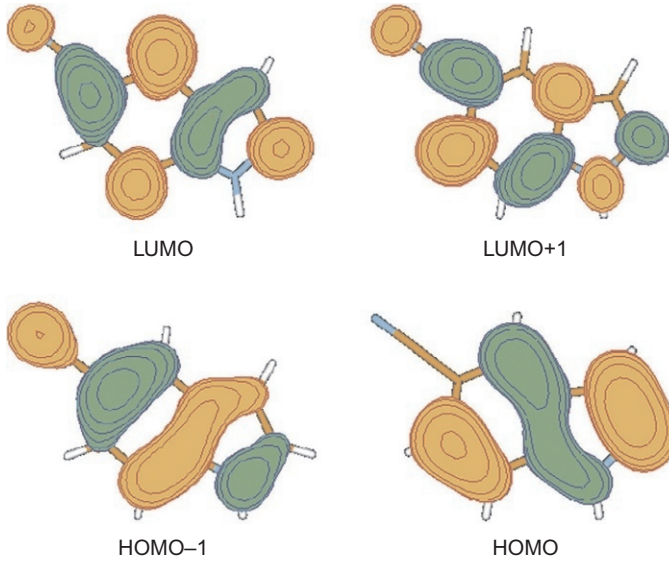

FIG. 26 Contour plots of the highest occupied and lowest unoccupied molecular orbitals of 5-cyanoindole at the optimized S_1 geometry from SCS-CC2/cc-pVTZ calculations, isosurface value 0.03.

of $0.77(\text{HOMO} \rightarrow \text{LUMO}) + 0.44(\text{HOMO} - 1 \rightarrow \text{LUMO}) - 0.29(\text{HOMO} \rightarrow \text{LUMO} + 1) - 0.26(\text{HOMO} - 2 \rightarrow \text{LUMO})$. The excitation to both states is therefore heavily mixed and the second excited singlet state is accompanied by a considerable charge migration from the indolic NH group to the cyano group.

Thus, from the comparison of both the transition dipole moment and the permanent excited state dipole moments, it can be concluded that the lowest excited singlet state of 5-cyanoindole is not a charge-transfer state, but a locally excited state, which has mixed L_a/L_b character.

8.4 Comparison of Excited State Dipole Moments From Gas Phase and Condensed Phase Experiments

The collection of excited state dipole moments, determined from rotationally resolved Stark spectra helps in the evaluation of solvent-based methods, which rely on spectral shifts. Unfortunately, the number of investigations using the Lippert-Mataga or similar approximations for small molecules, that have already been studied with high resolution spectroscopic Stark methods is very limited. Before we start with a detailed comparison of individual molecules we will resume shortly the results of the gas-phase determinations of excited state dipole moments with respect to approximations, that are used in the analysis of solvent-induced shifts of the absorption and emission spectra.

Referring to Table 1, for most of the systems studied in the gas phase with Stark spectroscopy, not only the magnitude of the dipole moment in both electronic states has been determined, but also their components on the main inertial axes. From these components, the direction of the dipole moments can be determined, and hence also the angle that the ground and excited state dipole moments make. These angles have variations between 0° (the direction of the dipole remains unchanged upon excitation) and 180° (complete reversal of the dipole moment). Of the 40 substances that have been listed in Table 1, 17 have angles larger than 10°. Thus, one important approximation in the derivation of the Lippert-Mataga equation (and of the related equations by Bilot-Kawski [149], Bakhshiev [150], and McRea [151] that the orientation of the dipole moment remains unchanged during excitation is not fulfilled for nearly half of the molecules.

A few of the molecules in Table 1 have two or more conformers, which are separated by small (torsional) barriers, that are easily overcome in solution at room temperature. While the dipole moments of the individual conformers in the gas phase might be very different[11], their dipole moments in solution may be averaged partially over all torsional angles, depending on how fast the reaction field follows the changing dipole moments.

Although, the basis for a comparison of the gas phase and the solution data is quite narrow (cf. Table 3), it is obvious that in all cases the changes of the magnitudes of dipole moments in solution exceeds that of Stark effect measurement by a factor of 2 at least in some cases more than a factor of 10. This deviation can be explained in many cases by field induced mixing of higher electronic states, which have a larger dipole moment of the state to be observed. This field induced mixing is caused by the huge electric fields of the Onsager reaction field of the solvent. Solvents with smaller polarizability should therefore be advantageous in principal.

ACKNOWLEDGMENTS

The financial support of the Deutsche Forschungsgemeinschaft (SCHM1043/12-3) is gratefully acknowledged. This work has only become possible through the work of many PhD students in our groups. The general set-up of the molecular beam machine and early versions of the fitting program were done by Arnim Westphal and Jochen Küpper. Improving modifications have been introduced by Marcel Böhm and Christian Ratzer. The Stark modifications have been implemented by Josefin Wilke and Martin Wilke.

11. The dipole moment of *cis*-3-aminophenol is three times larger, than that of *trans*-3-aminophenol, cf. Table 1. They are separated by a torsional barrier of the phenolic hydroxy group of 2.3 kcal/mol [152].

TABLE 3 Dipole Moments of Molecules in Their Ground (μ'') and Electronically Excited States (μ') and Their Difference $\Delta\mu$ From Electronic Stark Spectroscopy in the Gas Phase and From Solvatochromic or Thermochromic Shifts in Solution

	Gas Phase					Solution					
	μ''	μ'	$\Delta\mu$	θ	Ref.	μ''	$\lvert\Delta\mu\rvert$	Ref.	μ''	$\Delta\mu$	Ref.
4-Aminobenzoic acid	3.3	4.4	+1.1	4	[104]	2.94	3.4	[20]			
Aniline	1.13	2.80	+1.77	0	[106]		3.5	[29]	1.53	0.84	[23]
5-Cyanoindole	7.14	8.17	+1.03	1	[117]	–	7.98	[153]			
Indole	1.96	1.86	−0.11	13	[108]		1.04	[154]			
5-Methoxyindole	1.59	1.14	−0.45	53	[36]		1.1	[155]			
cis-2-Naphthol	1.01	1.17	+0.16	12	[113]	0.93	1.02	[156]	1.18	1.06	[156]
trans-2-Naphthol	1.36	1.44	+0.08	29	[122]	0.93	1.02	[156]	1.18	1.06	[156]

REFERENCES

[1] W.G.J. Hol, P.T. Van Duijnen, H.J.C. Berendsen, The α-helix dipole and the properties of proteins, Nature 273 (1978) 443–446.

[2] D.R. Ripoll, J.A. Vila, H.A. Scheraga, On the orientation of the backbone dipoles in native folds, Proc. Natl. Acad. Sci. U. S. A. 102 (2010) 7559–7564.

[3] T. Förster, Zwischenmolekulare Energiewanderung und Fluoreszenz, Ann. Phys. 437 (1948) 55–75.

[4] J. Lakowicz, Principles of Fluorescence Spectroscopy, second ed., Plenum, New York, USA, 1999.

[5] H. van Amerongen, L. Valkunas, R. van Grondelle, Photosynthetic Excitons, World Scientific Publishing, Singapore, 2000.

[6] C.H. Townes, A.L. Schawlow, Microwave Spectroscopy, Dover Publications, New York, 1975.

[7] H.A. Dijkerman, G. Ruitenberg, Determination of the dipole moment of OCS with a microwave absorption cavity, Chem. Phys. Lett. 3 (1969) 172–174.

[8] R.G. Shulman, C.H. Townes, Molecular dipole moments and Stark effects. II. Stark effects in OCS, Phys. Rev. 77 (1950) 500–506.

[9] J. Stark, Beobachtungen über den Effekt des elektrischen Feldes auf Spektrallinien I. Quereffekt, Ann. Phys. 43 (1914) 965–983.

[10] P. Suppan, Invited review solvatochromic shifts: the influence of the medium on the energy of electronic states, J. Photochem. Photobiol. A 50 (1990) 293.

[11] T. Abe, I. Iweibo, Comparison of the excited-state dipole moments and polarizabilities estimated from solvent spectral shifts with those from electrooptical measurements, Bull. Chem. Soc. Jpn. 58 (1984) 3415–3422.

[12] W. Liptay, Dipole Moments and Polarizabilities of Molecules in Excited Electronic States, vol. I, Academic Press, New York, 1974, pp. 129–229. Chapter 4.

[13] W. Liptay, Electrochromism and solvatochromism, Angew. Chem. 8 (1969) 177–188.

[14] E. Lippert, Dipolmoment und Elektronenstruktur von angeregten Molekülen, Z. Naturforsch. 10A (1955) 541.

[15] N. Mataga, Y. Kaifu, M. Koizumi, Solvent effects upon fluorescence spectra and the dipole moments of excited molecules, Bull. Chem. Soc. Jpn. 29 (1956) 465.

[16] N. Mataga, Y. Kaifu, M. Koizumi, Electric moments of molecules in liquids, J. Am. Chem. Soc. 58 (1936) 1486–1493.

[17] F.W. Fowler, A.R. Katritzky, R.J.D. Rutherford, The correlation of solvent effects on physical and chemical properties, J. Chem. Soc. B (1971) 460–469.

[18] R.W. Taft, J.-L.M. Abboud, M.J. Kamlet, M.H. Abraham, Linear solvation energy relations, J. Sol. Chem. 14 (1985) 153–186.

[19] T. Abe, Estimation of angles between ground- and excited-state dipole moments from solvent spectral frequency shifts, Bull. Chem. Soc. Jpn. 64 (1991) 3224–3228.

[20] E.G. Demissie, E.T. Mengesha, G.W. Woyessa, Modified solvatochromic equations for better estimation of ground and excited state dipole moments of p-aminobenzoicacid (PABA): accounting for real shape over hypothetical spherical solvent shell, J. Photochem. Photobiol. A: Chem. 337 (2016) 184–191, https://doi.org/10.1016/j.jphotochem.2016.12.034.

[21] J.R. Lombardi, Solvatochromic shifts: a reconsideration, J. Phys. Chem. A 102 (1998) 2817–2823.

[22] J.R. Lombardi, Solvatochromic shifts reconsidered: field-induced mixing in the nonlinear region and application to indole, J. Phys. Chem. A 103 (1999) 6335–6338.

[23] A. Kawski, B. Kuklinski, P. Bojarski, Dipole moment of aniline in the excited S_1 state from thermochromic effect on electronic spectra, Chem. Phys. Lett. 415 (2005) 251–255.
[24] A. Kawski, B. Kuklinski, P. Bojarski, Dipole moment of benzonitrile in its excited S_1 state from thermochromic shifts of fluorescence spectra, Chem. Phys. Lett. 419 (2006) 309–312.
[25] J.R. Lombardi, Dipole moments of the lowest singlet $\pi^* \leftarrow \pi$ states in phenol and aniline, J. Chem. Phys. 50 (1969) 3780–3783.
[26] J.R. Lombardi, Electric field induced perturbations in the ultraviolet spectrum of aniline. Vibronic origin of the perturbing state, J. Chem. Phys. 56 (1972) 2278–2281.
[27] J.R. Lombardi, Electric field induced perturbations in the $^1B_2^1 \leftarrow A_1$ transition of aniline, Chem. Phys. 28 (1978) 41–45.
[28] T.M. Korter, D.R. Borst, C.J. Butler, D.W. Pratt, Stark effects in gas-phase electronic spectra. Dipole moment of aniline in its excited S_1 state, J. Am. Chem. Soc. 123 (2001) 96–99.
[29] P. Suppan, Excited-state dipole moments from absorption/fluorescence solvatochromic ratios, Chem. Phys. Lett. 94 (1983) 272–275.
[30] R. Sampathkumar, C.A. Gonsago, Studies of ground state and first excited singlet state dipole moments of anilines, J. Chem. Pharm. Res. 6 (2014) 139–147.
[31] N.H. Ayachit, Excited-state dipole moments from absorption and fluorescence solvatochromic shifts—a better approach, Proc. Indiana Acad. Sci. 101 (1989) 269–271.
[32] L.S. Prabhumirashi, On estimating excited state dipole moments from solvent effects on electronic absorption spectra-drawbacks and improvement in the procedure, Spectrochim. Acta 39A (1983) 91–92.
[33] J.R. Lombardi, On the comparison of solvatochromic shifts with gas phase Stark effect measurements, Spectrochim. Acta 43A (1987) 1223–1324.
[34] D.E. Freeman, W. Klemperer, Electric dipole moment of the $^1A_2$ electronic state of formaldehyde, J. Chem. Phys. 45 (1966) 52–57.
[35] M. Okruss, R. Müller, A. Hese, High-resolution ultraviolet laser spectroscopy on jet-cooled benzene molecules: ground and excited electronic state polarizabilities determined from static Stark effect measurements, J. Chem. Phys. 110 (1999) 10393–10402.
[36] J. Wilke, M. Wilke, W.L. Meerts, M. Schmitt, Determination of ground and excited state dipole moments via electronic Stark spectroscopy: 5-methoxyindole, J. Chem. Phys. 144 (2016) 044201-1–044201-10.
[37] M. Brieger, A. Renn, A. Hese, A. Sodeik, The dipole moment of ^{7}LiH in the electronically excited $A^1\Sigma^+$ state, Chem. Phys. Lett. 76 (1980) 465–468.
[38] P.J. Brucat, R.N. Zare, Determination of the effective electric dipole moments of selected $NO_2^2B_2$ fine structure levels, Mol. Phys. 55 (1985) 277–285.
[39] P. Schmidt, H. Bitto, J.R. Huber, Excited state dipole moments in a polyatomic molecule determined by Stark quantum beat spectroscopy, J. Chem. Phys. 88 (1988) 696–704.
[40] N. Ohta, T. Tanaka, Stark quantum beats and electric dipole moment in the S_1 state of pyrimidine vapor, J. Chem. Phys. 99 (1993) 3312–3319.
[41] A.L. Surdo, Sul fenomeno analogo a quello di Zeeman nel campo elettrico, Rendiconti della Reale Accademia dei Lincei 22 (1913) 664–666.
[42] P. Zeeman, The effect of magnetisation on the nature of light emitted by a substance, Nature 55 (1897) 347.
[43] W. Voigt, Ueber das Elektrische Analogon des Zeemaneffectes, Ann. Phys. 4 (1901) 197–208.
[44] R.deL. Kronig, The dielectric constant of diatomic dipole-gases on the new quantum mechanics, Proc. Natl. Acad. Sci. U. S. A. 12 (1926) 488–493.
[45] R.deL. Kronig, The dielectric constant of symmetrical polyatomic dipole-gases on the new quantum mechanics, Proc. Natl. Acad. Sci. U. S. A. 12 (1926) 608–612.

[46] J. Hougen, B.M. DeKoven, The application of extended permutation-inversion groups to internal rotation of a symmetric rotor top in a symmetric or asymmetric rotor molecule, J. Mol. Spectrosc. 114 (1983) 375–391.
[47] H.C. Allen, P.C. Cross, Molecular Vib-Rotors, Wiley, New York, 1963.
[48] J.K.G. Watson, Determination of centrifugal distortion coefficients of asymmetric-top molecules. III. Sextic coefficients, J. Chem. Phys. 48 (1968) 4517.
[49] W. Gordy, R.L. Cook, Microwave Molecular Spectra, third ed., Wiley, New York, 1984.
[50] Y.-P. Chang, F. Filsinger, B.G. Sartakov, J. Küpper, CMIstark: python package for the Stark-effect calculation and symmetry classification of linear, symmetric and asymmetric top wavefunctions in dc electric fields, Comput. Phys. Commun. 185 (2014) 339–349.
[51] I. Ozier, W.L. Meerts, The Stark and Zeeman effects in methyl silane, J. Mol Spec. 93 (1982) 164–178.
[52] F.W. Loomis, R.W. Wood, The rotational structure of the blue-green bands of Na_2, Phys. Rev. 32 (1928) 223–236.
[53] T. Nakagawa, J. Overend, Computer-assisted assignment of vibration-rotation spectra, J. Mol. Spectrosc. 50 (1974) 333–348.
[54] J.F. Scott, K.N. Rao, Computer-assisted assignment of vibration-rotation spectra, J. Mol. Spectrosc. 20 (1966) 461–463.
[55] B. Winnewisser, J. Reinstädtler, Interactive Loomis-Wood assignment programs, J. Mol. Spectrosc. 136 (1989) 12–16.
[56] W. Łodyga, M. Kre¸glewski, P. Pracna, Š. Urban, Advanced graphical software for assignments of transitions in rovibrational spectra, J. Mol. Spectrosc. 243 (2007) 182–188.
[57] C.F. Neese, An interactive Loomis-Wood package for spectral assignment in IGOR pro, in: International Symposium on Molecular Spectroscopy, 56th Meeting, June 11–15, 2001.
[58] C.D. Thompson, E.G. Robertson, D. McNaughton, Reading between the lines: exposing underlying features of high resolution infrared spectra ($CHClF_2$), Phys. Chem. Chem. Phys. 5 (2003) 1996–2000.
[59] D.F. Plusquellic, R.D. Suenram, B. Mate, J.O. Jensen, A.C. Samuels, The conformational structures and dipole moments of ethyl sulfide in the gas phase, J. Chem. Phys. 115 (2001) 3057–3067.
[60] G. Moruzzi, A heuristic approach to automated molecular line assignment, J. Mol. Spectrosc. 229 (2005) 19–30.
[61] R.M. Helm, H.-P. Vogel, H.J. Neusser, Highly resolved UV spectroscopy: structure of S_1 benzonitrile and benzonitrile-argon by correlation automated rotational fitting, Chem. Phys. Lett. 270 (1997) 285–291.
[62] R.M. Helm, H.P. Vogel, H.J. Neusser, Rotational analysis and tunnel splittings of the intermolecular vibrations of the phenol-water complex by high resolution UV spectroscopy, J. Chem. Phys. 108 (1998) 4496–4504.
[63] C.M. Western, B.E. Billinghurst, Automatic assignment and fitting of spectra with pgopher. Phys. Chem. Chem. Phys. 19 (16) (2017) 10222–10226, https://doi.org/10.1039/c7cp00266a.
[64] J.H. Holland, Adaption in Natural and Artificial Systems, The University of Michigan Press, Ann Arbor, MI, 1975.
[65] I. Rechenberg, Evolutionsstrategie—Optimierung technischer Systeme nach Prinzipien der biologischen Evolution, Frommann-Holzboog, Stuttgart, 1973.
[66] H.-P. Schwevel, Evolution and Optimum Seeking, John Wiley & Son, New York, 1993.
[67] W.L. Meerts, M. Schmitt, G. Groenenboom, New applications of the genetic algorithm for the interpretation of high resolution spectra, Can. J. Chem. 82 (2004) 804–819.

[68] W.L. Meerts, M. Schmitt, A new automated assign and analyzing method for high resolution rotational resolved spectra using genetic algorithms, Phys. Scr. 73 (2005) C47–C52.
[69] W.L. Meerts, M. Schmitt, Application of genetic algorithms in automated assignments of high-resolution spectra, Int. Rev. Phys. Chem. 25 (2006) 353–406.
[70] M. Schmitt, W.L. Meerts, Rotationally resolved electronic spectroscopy and automatic assignment techniques using evolutionary algorithms, in: M. Quack, F. Merkt (Eds.), Handbook of High Resolution Spectroscopy, John Wiley and Sons, New York, 2011. ISBN: 978-0-470-06653-9.
[71] A. Ostermeier, A. Gawelczyk, N. Hansen, Step-size adaptation based on non-local use of selection information, in: Lecture Notes in Computer Science: Parallel Problem Solving from Nature (PPSN III), Springer-Verlag, London, UK, 1994, pp. 189–198.
[72] N. Hansen, A. Ostermeier, Completely derandomized self-adaptation in evolution strategies, Evol. Comput. 9 (2) (2001) 159–195.
[73] N. Hansen, S. Kern, Evaluating the CMA evolution strategy on multimodal test functions, in: X. Yao (Ed.), LNCS, Parallel Problem Solving from Nature PPSN VIII, vol. 3242, Springer, Berlin/Heidelberg, 2004, , pp. 282–291.
[74] A. Altay, G. Kayakutlu, Y.I. Topcu, Win-win match using a genetic algorithm, Appl. Math. Mod. 34 (2010) 2749–2762.
[75] C. Garuti, V.A.P. Salomon, Compatibility indices between priority vectors, Int. J. Anal. Hierarchy Process 4 (2012) 152–160.
[76] T.L. Saaty, A ratio scale metric and the compatibility of ratio scales: the possibility of arrow's impossibility theorem, Appl. Math. Lett. 7 (1994) 51–57.
[77] K. Pearson, Notes on regression and inheritance in the case of two parents, Proc. R. Soc. Lond. 58 (1895) 240–242.
[78] J.A. Hageman, R. Wehrens, R. de Gelder, W.L. Meerts, L.M.C. Buydens, Direct determination of molecular constants from rovibronic spectra with genetic algorithms, J. Chem. Phys. 113 (2000) 7955–7962.
[79] W.A. Majewski, W.L. Meerts, Near UV spectra with fully resolved structure of naphthalene and perdeuterated naphthalene, J. Mol. Spectrosc. 104 (1984) 271–281.
[80] W.A. Majewski, D.F. Plusquellic, D.W. Pratt, The rotationally resolved fluorescence excitation spectrum of 1-fluoronaphthalene, J. Chem. Phys. 90 (1989) 1362–1367.
[81] M. Schmitt, J. Küpper, D. Spangenberg, A. Westphal, Determination of the structures and barriers to hindered internal rotation of the phenol-methanol cluster in the S_0 and S_1 state, Chem. Phys. 254 (2000) 349–361.
[82] J. Ross (Ed.), Molecular beams, in: Advances in Chemical Physics, Interscience Publishers, New York, London, Sydney, 1966.
[83] G. Scoles, Atomic and Molecular Beam Methods, vol. 1, Oxford University Press, New York, Oxford, 1988.
[84] J.M.L.J. Reinartz, A. Dymanus, Molecular constants of OCS isotopes in the $(01^{1}0)$ vibrational state measured by molecular-beam electric-resonance, Chem. Phys. Lett. 24 (1974) 346–351.
[85] K. Wohlfart, M. Schnell, J.U. Grabow, J. Küpper, Precise dipole moment and quadrupole coupling constants of benzonitrile, J. Mol. Spectrosc. 247 (2014) 119–121.
[86] G.W. Parker, Electric field outside a parallel plate capacitor, Am. J. Phys. 70 (5) (2002) 502–507.
[87] P.M. Felker, Rotational coherence spectroscopy: studies of the geometries of large gas-phase species by picosecond time-domain methods, J. Phys. Chem. 96 (1992) 7844–7857.
[88] C. Riehn, High-resolution pump-probe rotational coherence spectroscopy—rotational constants and structure of ground and electronically excited states of large molecular systems, Chem. Phys. 297 (2002) 283.

[89] H.-M. Frey, D. Kummli, S. Lobsiger, S. Leutwyler, High-Resolution Rotational Raman Coherence Spectroscopy with Femtosecond Pulses, John Wiley & Sons, Ltd, New York, 2011. https://doi.org/10.1002/9780470749593.hrs055.

[90] D.S. Kummli, S. Lobsiger, H.-M. Frey, S. Leutwyler, J.F. Stanton, Accurate determination of the structure of cyclooctatetraene by femtosecond rotational coherence spectroscopy and ab initio calculations, J. Phys. Chem. A 112 (38) (2008) 9134–9143.

[91] D.E. Freeman, J.R. Lombardi, W. Klemperer, Electric dipole moment of the lowest singlet π^*-n state of propynal, J. Chem. Phys. 45 (1966) 58–60.

[92] J.R. Lombardi, D. Campbell, W. Klemperer, Electric dipole moment of the $n-\pi^*$ singlet state of HCOF, J. Chem. Phys. 46 (1967) 3482–3486.

[93] J.R. Lombardi, W. Klemperer, M.B. Robin, H. Basch, N.A. Kuebler, Optical spectra of small rings. I. The $n \rightarrow \pi^*$ transition of difluorodiazirine, J. Chem. Phys. 51 (1969) 33–44.

[94] K.-T. Huang, J.R. Lombardi, Dipole moment of the first excited singlet $\pi^* \leftarrow \pi$ state in fluorobenzene, J. Chem. Phys. 52 (1970) 5613–5615.

[95] C.Y. Wu, J.R. Lombardi, Dipole moment in the lowest $^1B_2$ state of chlorobenzene, J. Chem. Phys. 55 (1971) 1997–1998.

[96] H. Parker, J.R. Lombardi, Dipole moment of the first excited $\pi^* \leftarrow \pi$ state of styrene, J. Chem. Phys. 54 (1971) 5095–5096.

[97] M. Okruss, R. Müller, A. Hese, High-resolution ultraviolet laser spectroscopy on jet-cooled benzene molecules: ground and excited electronic state polarizabilities determined from static Stark effect measurements, J. Chem. Phys. 110 (21) (1999) 10393–10402.

[98] M. Okruss, F. Penn, A. Hese, Stark effect and fluorescence quenching in the $S_1 \leftarrow S_0 0_0^0$ rovibronic spectrum of pyrazine, J. Mol. Struct. 348 (1995) 119–122.

[99] V. Bendkowsky, E. Heinecke, A. Hese, High-resolution laser spectroscopy on the $S_1 \leftarrow S_0$ transition of jet-cooled anthracene: rotational structure and Stark effect, J. Chem. Phys. 127 (22) (2007) 224306-1–224306-5.

[100] E. Heinecke, D. Hartmann, A. Hese, Laser spectroscopy of free pentacene molecules (II): Stark effect of the vibrationless $S_1 \leftarrow S_0$ transition, J. Chem. Phys. 118 (1) (2003) 113–120.

[101] M. Okruss, B. Rosenow, A. Hese, Electric properties of organic molecules. The ground and excited vibronic state dipole moments of 1-fluoronaphthalene, Chem. Phys. Lett. 220 (1994) 286.

[102] M. Okruss, Rotationsstruktur- und Starkeffektuntersuchungen an ausgewählten aromatischen Molekülen im Überschalldüsenstrahl mittels hochauflösender UV-Laserspektroskopie, Dissertation, Technische Universität, Berlin, 2005.

[103] J.A. Reese, T.V. Nguyen, T.M. Korter, D.W. Pratt, Charge redistribution on electronic excitation. Dipole moments of cis- and trans-3-aminophenol in their S_0 and S_1 electronic states, J. Am. Chem. Soc. 126 (2004) 11387–11392.

[104] D.M. Mitchell, P.J. Morgan, D.W. Pratt, Push-pull molecules in the gas phase: Stark-effect measurements of the permanent dipole moments of p-aminobenzoic acid in its ground and electronically excited states, J. Phys. Chem. A 112 (49) (2008) 12597–12601.

[105] D.M. Miller, P.J. Morgan, D.W. Pratt, On the electric dipole moments of asymmetric tops: measurement by high-resolution electronic spectroscopy in the gas phase, J. Phys. Chem. A 113 (25) (2009) 6964–6970, https://doi.org/10.1021/jp9017585.

[106] D.R. Borst, T.M. Korter, D.W. Pratt, On the additivity of bond dipole moments. Stark effect studies of the rotationally resolved electronic spectra of aniline, benzonitrile and aminobenzonitrile, Chem. Phys. Lett. 350 (2001) 485–490.

[107] D.R. Borst, D.W. Pratt, M. Schafer, Molecular recognition in the gas phase. Dipole-bound complexes of benzonitrile with water, ammonia, methanol, acetonitrile, and benzonitrile itself, Phys. Chem. Chem. Phys. 9 (32) (2007) 4563–4571.

[108] C. Kang, T.M. Korter, D.W. Pratt, Experimental measurement of the induced dipole moment of an isolated molecule in its ground and electronically excited states: indole and indole-H_2O, J. Chem. Phys. 122 (2005) 174301.

[109] A.J. Fleisher, J.W. Young, D.W. Pratt, Experimentally measured permanent dipoles induced by hydrogen bonding. The Stark spectrum of indole-NH_3, Phys. Chem. Chem. Phys. 14 (25) (2012) 8990–8998.

[110] C. Kang, J.T. Yi, D.W. Pratt, Stark effects in the gas phase: dipole moment of 7-azaindole in its ground and electronically excited states, Chem. Phys. Lett. 423 (1–3) (2006) 7–12.

[111] J.W. Young, Z.D. Pozun, K.D. Jordan, D.W. Pratt, Excited electronic state mixing in 7-azaindole. Quantitative measurements using the Stark effect, J. Phys. Chem. B 117 (49) (2013) 15695–15700.

[112] T.V. Nguyen, D.W. Pratt, Permanent electric dipole moments of four tryptamine conformers in the gas phase: a new diagnostic of structure and dynamics, J. Chem. Phys. 124 (5) (2006) 054317.

[113] A.J. Fleisher, P.J. Morgan, D.W. Pratt, Charge transfer by electronic excitation: direct measurement by high resolution spectroscopy in the gas phase, J. Chem. Phys. 131 (21) (2009) 211101.

[114] A.J. Fleisher, J.W. Young, D.W. Pratt, A. Cembran, J. Gao, Flickering dipoles in the gas phase: structures, internal dynamics, and dipole moments of β-naphthol-H_2O in its ground and excited electronic states, J. Chem. Phys. 134 (11) (2011) 114304.

[115] J.A. Thomas, J.W. Young, A.J. Fleisher, L. Alvarez-Valtierra, D.W. Pratt, Stark-effect studies of 1-phenylpyrrole in the gas phase. Dipole reversal upon electronic excitation, J. Phys. Chem. Lett. 1 (13) (2010) 2017–2019.

[116] J.W. Young, V. Vaquero-Vara, J.T. Yi, D.W. Pratt, G. Moreno-Vargas, L. Alvarez-Valtierra, Using high resolution electronic spectroscopy to probe the effects of ring twist on charge transfer in 2-phenylindole and N-phenylcarbazole, Phys. Chem. Chem. Phys. 15 (25) (2013) 10251–10257.

[117] J. Wilke, M. Wilke, C. Brand, W.L. Meerts, M. Schmitt, On the additivity of molecular fragment dipole moments of 5-substituted indole derivatives, ChemPhysChem 17 (17) (2016) 2736–2743.

[118] M. Schneider, M. Wilke, M.L. Hebestreit, M. Schmitt, Dipole moments of 1,3-dimethoxybenzene from rotationally resolved Stark spectroscopy, unpublished data.

[119] J. Wilke, M. Wilke, C. Brand, J.D. Spiegel, C.M. Marian, M. Schmitt, Modulation of the L_a/L_b mixing in an indole derivative: a position-dependent study using 4-, 5-, and 6-fluoroindole, J. Phys. Chem. A 121 (2017) 1597–1608.

[120] A.J. Fleisher, J.W. Young, D.W. Pratt, Experimentally measured permanent dipoles induced by hydrogen bonding. The Stark spectrum of indole-NH_3, Phys. Chem. Chem. Phys. 14 (2012) 8990–8998.

[121] M. Wilke, C. Brand, J. Wilke, M. Schmitt, Influence of the position of the methoxy group on the stabilities of the syn and anti conformers of 4-, 5-, and 6-methoxyindole, J. Mol. Spectrosc. 337 (2017) 137–144.

[122] A.J. Fleisher, J.W. Young, D.W. Pratt, A. Cembran, J. Gao, Flickering dipoles in the gas phase: structures, internal dynamics, and dipole moments of β-naphthol-H_2O in its ground and excited electronic states, J. Chem. Phys. 134 (2011) 114304-1–114304-12.

[123] T.V. Nguyen, D.W. Pratt, Permanent electric dipole moments of four tryptamine conformers in the gas phase: a new diagnostic of structure and dynamics, J. Chem. Phys. 124 (2006) 054317.

[124] D.R. Lide, CRC Handbook of Chemistry and Physics, 85th ed., CRC Press, New York, USA, 2004.

[125] L. Nygaard, E.R. Hansen, R.L. Hansen, J. Rastrup-Andersen, G.O. Sorensen, Microwave spectra and dipole moments of 1,2-difluorobenzene and 1,3-difluorobenzene, Spectrochim. Acta 23 A (1967) 2813–2819.
[126] J.R. Platt, Classification of spectra of cata-condensed hydrocarbons, J. Chem. Phys. 17 (1949) 484–495.
[127] G. Weber, Fluorescence-polarization spectrum and electronic-energy transfer in tyrosine, tryptophan and related compounds, Biochem. J. 75 (1960) 335–345.
[128] T. Tripathy, B.R. De, Making sense about dipole moments, J. Phys. Sci. 12 (2008) 155–172.
[129] C. Brand, O. Oeltermann, M. Wilke, J. Tatchen, M. Schmitt, Ground and electronically excited singlet state structures of 5-fluoroindole, deduced from rotationally resolved electronic spectroscopy and *ab initio* theory, ChemPhysChem 13 (2012) 3134–3138.
[130] G. Berden, W.L. Meerts, M. Schmitt, K. Kleinermanns, High resolution UV spectroscopy of phenol and the hydrogen bonded phenol-water cluster, J. Chem. Phys. 104 (1996) 972–982.
[131] J.W. Ribblett, W.E. Sinclair, D.R. Borst, J.T. Yi, D.W. Pratt, High resolution electronic spectra of anisole and anisole-water in the gas phase: hydrogen bond switching in the S_1 state, J. Phys. Chem. A 110 (2006) 1478–1483.
[132] A.E. Reed, R.B. Weinstock, F. Weinhold, Natural population analysis, J. Chem. Phys. 83 (1985) 735–746.
[133] W. Rettig, F. Marschner, Population of excited charge transfer states and molecular conformation in N-phenylpyrrole, Nouv. J. Chim. 7 (1983) 425–431.
[134] K.A. Zachariasse, Comment on "Pseudo-Jahn-Teller and TICT models: a photophysical comparison of meta- and para-DMABN derivatives" J. Phys. Chem. Lett. 320 (2000) 8–13.
[135] O. Desyatnyk, L. Pszczolkowski, S. Thorwirth, T.M. Krygowski, Z. Kisiel, The rotational spectra electric dipole moments and molecular structures of anisole and benzaldehyde, Phys. Chem. Chem. Phys. 7 (2005) 1708–1715.
[136] P.R. Callis, ^1L_a and ^1L_b transitions of tryptophan: applications of theory and experimental observations to fluorescence of proteins, in: L. Brand, M.L. Johnson (Eds.), Methods in Enzymology, vol. 278, Academic Press, San Diego, CA, 1997, pp. 113–150.
[137] C. Brand, J. Küpper, D.W. Pratt, W.L. Meerts, D. Krügler, J. Tatchen, M. Schmitt, Vibronic coupling in indole: I. Theoretical description of ^1L_a and ^1L_b interactions and the absorption spectrum, Phys. Chem. Chem. Phys. 12 (2010) 4968–4997.
[138] J. Küpper, D.W. Pratt, W.L. Meerts, C. Brand, J. Tatchen, M. Schmitt, Vibronic coupling in indole: II. Investigation of the ^1L_a-^1L_b interaction using rotationally resolved electronic spectroscopy, Phys. Chem. Chem. Phys. 12 (2010) 4980–4988.
[139] O. Oeltermann, C. Brand, B. Engels, J. Tatchen, M. Schmitt, The structure of 5-cyanoindole in the ground and lowest electronically excited singlet state, deduced from rotationally resolved electronic spectroscopy and ab initio theory, Phys. Chem. Chem. Phys. 14 (2012) 10266–10270.
[140] O. Oeltermann, C. Brand, W.L. Meerts, J. Tatchen, M. Schmitt, Rotationally resolved electronic spectroscopy of 2,3-bridged indole derivatives: tetrahydrocarbazole, J. Mol. Struct. 933 (2011) 2–8.
[141] C. Brand, O. Oeltermann, D.W. Pratt, R. Weinkauf, W.L. Meerts, W. van der Zande, K. Kleinermanns, M. Schmitt, Rotationally resolved electronic spectroscopy of 5-methoxyindole, J. Chem. Phys. 133 (2010) 024303-1–024303-11.
[142] C. Brand, O. Oeltermann, M. Wilke, M. Schmitt, Position matters: high resolution spectroscopy on 6-methoxyindole, J. Chem. Phys. 138 (2013) 024321.

[143] B. Albinsson, B. Nordén, Excited-state properties of the indole chromophore—electronic-transition moment directions from linear dichroism measurements—effect of methyl and methoxy substituents, J. Phys. Chem. 96 (1992) 6204.
[144] M.R. Eftink, L.A. Selvidge, P.R. Callis, A.A. Rehms, Photophysics of indole derivatives: experimental resolution of L_a and L_b transitions and comparison with theory, J. Phys. Chem. 94 (1990) 3469–3479.
[145] M. Martinaud, A. Kadiri, Comparative sensibility of the $S_1 \leftarrow S_0$ and $S_2 \leftarrow S_0$ indole electronic transitions to environment perturbations. The position of the 0-0 bands in polar media, Chem. Phys. 28 (1978) 473–485.
[146] C. Hättig, F. Weigend, CC2 excitation energy calculations on large molecules using the resolution of the identity approximation, J. Chem. Phys. 113 (2000) 5154–5161.
[147] C. Hättig, A. Köhn, Transition moments and excited-state first-order properties in the coupled cluster model CC2 using the resolution-of-the-identity approximation, J. Chem. Phys. 117 (2002) 6939–6951.
[148] C. Hättig, Geometry optimizations with the coupled-cluster model CC2 using the resolution-of-the-identity approximation, J. Chem. Phys. 118 (2002) 7751–7761.
[149] L. Bilot, A. Kawski, Zur Theorie des Einflusses von Lösungsmitteln auf die Elektronenspektren der Moleküle, Z. Naturforsch. 17A (1962) 621–627.
[150] N.G. Bakhshiev, Universal intermolecular interactions and their effect on the position of the electronic spectra of molecules in two component solutions, Opt. Spectrosk. 13 (1962) 24–29.
[151] E.M. Rae, Theory of solvent effects on molecular electronic spectra. Frequency shifts, J. Phys. Chem. 61 (1957) 562–572.
[152] W.Y. Sohn, M. Kim, S.-S. Kim, Y.D. Park, H. Kang, Solvent-assisted conformational isomerization and the conformationally-pure REMPI spectrum of 3-aminophenol, Phys. Chem. Chem. Phys. 13 (2011) 7037–7042.
[153] M. Sun, The excited state dipole moments and high resolution luminescence spectroscopy of indoles, PhD Thesis, Texas Tech University, 1974.
[154] A. Kawski, Thermochromic shifts of electronic spectra and excited state dipole moments, Asian J. Spectrosc. 1 (1997) 27–38.
[155] M.V. Hershberger, R.W. Lumry, The photophysics of 5-methoxyindole. A non-exciplex forming indole: additional evidence for two classes of exciplexes, Photochem. Photobiol. 23 (1994) 391–397.
[156] R. Gahlaut, N. Tewari, J.P. Bridhkoti, N.K. Joshi, H.C. Joshi, S. Pant, Determination of ground and excited state dipole moments of some naphthols using solvatochromic shift method, J. Mol. Liq. 163 (2011) 141–146.